



Review

Vanadium complexes immobilized on solid supports and their use as catalysts for oxidation and functionalization of alkanes and alkenes

Mannar R. Maurya^{a,*}, Amit Kumar^b, J. Costa Pessoa^{b,**}^a Department of Chemistry, Indian Institute of Technology Roorkee, Roorkee 247667, India^b Centro Química Estrutural, Instituto Superior Técnico, TU Lisbon, Av Rovisco Pais, 1049-001 Lisboa, Portugal

Contents

1. Introduction.....	2316
2. Immobilization of vanadium complexes	2317
2.1. Immobilization of vanadium complexes on polymer supports.....	2317
2.2. Encapsulation of vanadium complexes in zeolite-NaY	2321
2.3. Immobilization of vanadium complexes on ordered mesoporous silicas.....	2323
3. Characterization methods	2325
3.1. Analytical data.....	2325
3.2. IR and Raman spectroscopy	2326
3.3. Thermogravimetric analysis.....	2327
3.4. Adsorption studies	2327
3.5. Powder X-ray diffraction.....	2328
3.6. Field emission-scanning electron microscope (FE-SEM) and X-ray fluorescence (XRF) studies.....	2328
3.7. X-ray absorption spectroscopy	2329
3.8. Electronic spectroscopy	2329
3.9. EPR spectroscopy	2330
3.10. Magnetic properties.....	2331
3.11. Solid state NMR spectroscopy	2331

Abbreviations: AAS, atomic absorption spectroscopy; AES, Auger electron spectroscopy; [14]aneN₄ ligands, tetraaza-2,9-dioxo-4,11-diphenylcyclotetradecane ligands; [14]aneN₄, 1,5,8,12-tetraaza-2,9-dioxo-4,11-diphenylcyclotetradecane; [16]aneN₄ ligands, tetraaza-2,10-dioxo-4,12-diphenylcyclohexadecane ligands; Bzo₂[14]aneN₄, dibenzo-1,5,8,12-tetraaza-2,9-dioxo-4,11-diphenylcyclotetradecane; [16]aneN₄, 1,5,9,13-tetraaza-2,10-dioxo-4,12-diphenylcyclohexadecane; Bzo₂[16]aneN₄, dibenzo-1,5,9,13-tetraaza-2,10-dioxo-4,12-diphenylcyclohexadecane; APTS, 3-aminopropyltrimethoxysilane; APES, 3-aminopropyltriethoxysilane; BET, Brunauer, Emmett and Teller method (adsorption studies); BJH, Barrett–Joyner–Halenda method (adsorption studies); CPTMS, chloropropyltetramethylsilane; 3-CPTES, 3-chloropropyltetraethylsilane; CP-MCM-41, MCM-41 modified with chloropropyltetramethylsilane; CP-MAS NMR, cross-polarization magic angle spinning NMR spectroscopy; ct transitions, charge transfer transitions; DAB, 1,4-diazabutadiene; DRS, diffuse reflectance spectra; EDX or EDS, energy dispersive X-ray analysis; e.e., enantiomeric excess; EPR, electron paramagnetic resonance; EXAFS, extended X-ray absorption fine structure; FE-SEM, field emission-scanning electron microscope; FL, flexible ligand method; H₂fsal-β-Ala, Schiff base derived from 3-formylsalicylic acid and β-alanine; H₂fsal-amp, Schiff base derived from 3-formylsalicylic acid and 2-amino-2-methylpropanol.; H₂fsal-dmen, Schiff base derived from 3-formylsalicylic acid and N,N-dimethyl ethylenediamine; H₂fsal-aepy, Schiff base derived from 3-formylsalicylic acid and 2-aminoethylpyridine; H₂fsal-pa, Schiff base derived from 3-formylsalicylic acid and 3-aminopropanol.; H₂fsal-ea, Schiff base derived from 3-formylsalicylic acid and 2-aminoethanol; hmbmz, 2-hydroxymethylbenzimidazole; hpbmz, 2-(2-hydrpxyphenyl)benzimidazole; ICP, inductively coupled plasma; IM, impregnation method; lmct, ligand to metal charge transfer transitions; MAS, magic angle spinning; MCM-41, mobile crystalline material number 41; 2-pybmz, 2-(2-pyridyl)benzimidazole; 3-pybmz, 2-(3-pyridyl)benzimidazole; Pc, phthalocyanine ligand; PS-CH₂-Cl, chloromethylated polystyrene cross-linked with divinyl benzene; Hsal-ambmz, Schiff base derived from salicylaldehyde and 2-aminomethylbenzimidazole; H₂sal-bhz, Schiff base derived from salicylaldehyde and benzoylhydrazide; H₂sal-inh, Schiff base derived from salicylaldehyde and isonicotinic acid hydrazide; H₂sal-ohyba, Schiff base derived from salicylaldehyde and o-hydroxybenzylamine; H₂sal-pheol, Schiff base derived from salicylaldehyde and L-phenylalaninol; H₂sal-hisol, Schiff base derived from salicylaldehyde and L-histidinol; H₂sal-hist, Schiff base derived from salicylaldehyde and histidine; H₂sal-oaba, Schiff base derived from salicylaldehyde and o-aminobenzyl alcohol; H₂sal-phe, Schiff base derived from salicylaldehyde and L-phenylalanine; H₂sal-ea, Schiff base derived from salicylaldehyde and 2-aminoethanol; SB, ship-in-a-bottle; TBHP, t-butylhydroperoxide; tmbmz, thiomethylbenzimidazole; TOF, turn over frequency; TON, turn over number; TEOS, tetraethylorthosilicate; TGA or TG, thermogravimetric analysis; TS, template synthesis method; V-MCM-41, MCM-41 modified with a vanadium compound; V^{IV}O(bipy)₂²⁺, bis-bipyridyl oxidovanadium(IV); V^{IV}O(salen), N,N'-ethylenebis(salicylidene amino) oxidovanadium(IV); V^{IV}O(saloph), N,N'-o-phenylenebis(salicylidene amino) oxidovanadium(IV); V^{IV}O(Salten), N,N'-bis(salicylidene)diethylenetriamine oxidovanadium(IV); V^{IV}O(pic)₂, bis-picolinato oxidovanadium(IV); VBrPO, vanadium bromoperoxidases; V-HalPO, vanadate-dependent haloperoxidases; UHP, urea hydroperoxide; X₂-haacac, tetradentate Schiff-base ligands derived from acetylacetone and x-substituted o-aminophenol; XAS, X-ray absorption spectroscopy; XPS, X-ray photoelectron spectroscopy; XRD, X-ray diffraction; XANES, X-ray absorption near edge structure; XRF, X-ray fluorescence.

* Corresponding author. Tel.: +91 1332 285327; fax: +91 1332 273560.

** Corresponding author. Tel.: +351 218419268; fax: +351 218464455.

E-mail addresses: rkanficy@iitr.ernet.in (M.R. Maurya), joao.pessoa@ist.utl.pt (J. Costa Pessoa).

4. Catalytic activity studies.....	2332
4.1. Oxidative halogenation.....	2332
4.2. Oxidation of organic sulfides.....	2332
4.3. Oxidation of phenol.....	2333
4.4. Hydroamination and oxidative amination.....	2335
4.5. Oxidation of styrene.....	2337
4.6. Oxidation of <i>trans</i> -stilbene, isosafrol and geraniol.....	2337
4.7. Oxidation of cyclohexene, cyclooctene and limonene.....	2338
4.8. Oxidation of benzoin.....	2339
4.9. Oxidation of cyclohexane.....	2340
4.10. Oxidation of adamantane.....	2340
4.11. Oxidation of benzene, naphthalene, cumene, <i>p</i> -chlorotoluene and ethylbenzene.....	2340
4.12. Oxidation of alkanes.....	2341
4.13. Oxidation of α -hydroxy esters.....	2341
4.14. Formation of cyanohydrins.....	2342
5. Concluding remarks.....	2342
Acknowledgments.....	2343
References.....	2343

ARTICLE INFO

Article history:

Received 8 November 2010

Accepted 28 January 2011

Available online 5 March 2011

Keywords:

Supported vanadium complexes

Polymer-support

Zeolite-Y encapsulated complexes

MCM-supported complexes

Catalysts

Organic transformations

ABSTRACT

This review mainly discusses the immobilization strategies that have been used for vanadium complexes, typically mesoporous material, zeolites and polymers, the characterization procedures for the obtained materials, and their catalytic applications. The retention of the active metal compound within the catalyst may be based on (i) adsorption, (ii) the formation of covalent bonds between metal ligand and support, (iii) ion exchange, (iv) encapsulation, or (v) entrapment. The heterogenized complexes are used as catalysts for oxidations and functionalization of alkanes, alkenes and other substrates, and an account of the various applications reported is given.

© 2011 Elsevier B.V. All rights reserved.

1. Introduction

Catalysts have played a vital role in organic transformations and have major impact on the quality of human life as well as on economic progress. More than 90% of the processes in the petroleum, petrochemical, fertilizers and food industries are catalytically induced. While heterogeneous catalysis is preferred for commodity materials, most of the catalytic processes widely engaged in the manufacture of bulk as well as fine chemicals are homogenous in nature, producing large amount of side waste materials and imposing hazardous impact on the surrounding environment.

One of the major drawbacks of the homogeneous catalysts is the difficulty in separating the relatively expensive catalysts from the reaction mixture at the end of the process. The possible contamination of catalyst in the product also restricts their use in industry. Efficient anchoring of these catalysts on supports may overcome these drawbacks [1]. Since the catalytic action occurs at specific sites on the solid surface, often called as “active sites”, the uniform dispersion of metal catalysts is highly desirable for significant improvement of catalytic action. The inherent advantage of heterogeneous catalytic systems in the liquid phase over their homogeneous counterparts lies mainly on their easy separation and recycle ability. Various methodologies have been developed for the immobilization of homogeneous transition metal complexes. Organic polymers or inorganic solids like zeolites/molecular sieves, silica, alumina, other metal oxides, and carbon have been used as supports for the heterogenization of homogeneous catalysts.

The discovery of vanadate-dependent enzymes and their importance in various biological catalytic processes [2,3] has stimulated research on the catalytic aspects of vanadium complexes. Many model vanadium complexes show catalytic activity towards var-

ious organic transformations [4–10]. In search of catalysts for organic transformations we have directed our research on the immobilization of complexes on various solid supports. As benefits of this process, in many cases these catalysts (or catalyst precursors) are more active and easily recyclable, and maintain their activity after several cycles of catalytic use. In addition these catalysts exhibit increased stability and improved selectivity, which is ascribed to contributions of site-isolation and confinement effects, as well as cooperation effects from the support.

Heterogenization of catalysts has been the subject of an enormous number of publications, several reviews have been written on this topic [11–13]. Reviews have addressed catalytic applications of polystyrene-supported ligands and metal complexes [14–16], zeolite and ordered mesoporous molecular sieves as catalysts supports [13,17,19] and immobilized asymmetric catalysts [12,18,20,21]. In view of these, we present here a comprehensive overview of the vanadium complexes supported on cross-linked polystyrene, zeolites (mainly zeolite-NaY) and mesoporous materials (mainly MCM-41).

Four main distinct methodologies developed for the heterogenization of homogeneous catalysts, or the creation of heterogeneous catalysts, are: adsorption, encapsulation, covalent tethering and electrostatic interaction.

Catalysts immobilized by *adsorption* rely only on van der Waals interaction between the catalyst and the support. This is a weak interaction and the stability of the supported catalyst can be improved by modifying the catalyst and support to allow hydrogen bonding to occur.

Encapsulation is a process that does not require interactions between the catalyst and the support, and thus this method mimics the homogeneously catalyzed reactions. Other methods lead to changes in the catalyst. In fact, covalent tethering implies a

modification of the ligand, which may influence its electronic character and/or its conformation, and physisorption and ion-exchange methods result in the catalyst being in close proximity to the support which may also affect electronic properties and ligand conformation. To satisfy the condition of encapsulation, the catalyst must be larger than the pores of the support material to prevent loss of the catalyst into solution during the course of the reaction, or recovery process. As the catalyst complex is larger than the pores of the support, techniques such as impregnation cannot be used to synthesize these catalysts. The supported catalyst can be prepared by either (i) assembling the catalyst within the pores of the support or (ii) assembling the support around the catalyst.

Immobilization of complexes using *covalent tethering* techniques is the most favored approach to design stable heterogeneous catalysts. Different strategies have been developed depending upon the reaction being catalyzed and several examples are described below. Additionally many porous solids, including zeolites and ordered mesoporous silicates can act as ion exchangers. This presents a mechanism for the immobilization of metal cations and complexes through *electrostatic interaction*.

Of these four strategies immobilizations by covalent tethering and electrostatic interaction form reasonably stable catalysts that are capable of reuse. Adsorption methodologies are a simple method of immobilization but tend to produce non-stable catalysts. Encapsulation of complexes during the preparation methods provides a very elegant methodology but often it is relatively complex compared with the more recently developed covalent grafting methods [20]. Immobilization via ionic interaction is conceptually simple and may be a useful method of immobilizing ionic catalysts.

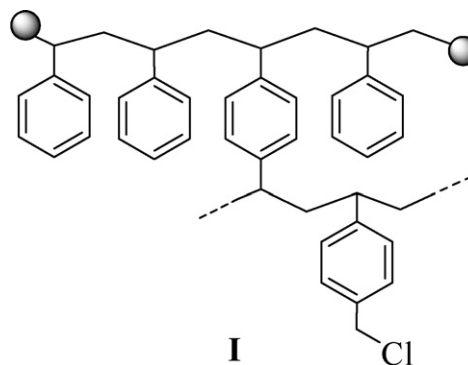
Many early studies concerned with immobilization of asymmetric homogeneous catalysts showed that lower yields and selectivity and/or enantioselectivity were achieved with the corresponding immobilized catalysts. However, more recent studies have shown this need not be the case. Indeed, some homogeneous systems have been shown to be much more enantioselective when immobilized. Among other aspects, the reasons for this change are site isolation effects, achievable through the appropriate design of immobilized catalysts, and the containment (or confinement) effect i.e. the immobilized catalyst is constrained through interaction with the supporting matrix, and this can induce increased selectivity and/or enantioselectivity compared with the corresponding homogeneous catalyst [20].

2. Immobilization of vanadium complexes

2.1. Immobilization of vanadium complexes on polymer supports

Many polymers are non-reactive, but they can be made reactive by imparting a functionality. Thus, polymers bearing a reactive functional group are called functionalized polymers. Synthesis of polypeptide chains over chloromethylated polystyrene by Merrifield in 1963 [22] has inspired researchers to develop new polymer-supported catalyst. Various polymers such as polystyrene, polyvinylchloride, polyvinylpyridine, polyaniline, polyallyl, polyaminoacid, acrylic polymer, cellulose, silicate are capable of undergoing a variety of chemical reactions and thus can be functionalized. The Merrifield resin (chloromethylated polystyrene cross-linked with divinyl benzene, hereafter designated by PS-CH₂-Cl or PS-MeCl) is the most widely used functional resin. Its structure is shown in Scheme 1 [23].

The functionalized polymers (cross-linked as well as straight chain) have widely been used as support for homogeneous catalysts through covalent bonding and many polymer-anchored ligands and their metal complexes have been synthesized by the stepwise modification of functionalized polymers. Generally, the organic



Scheme 1. Chloromethylated polystyrene cross-linked with divinylbenzene. The ball represents the backbone of polymer matrix.

reagents (ligands) react with the functionalized polymer to yield the polymer-bound reagents or ligands having available coordination sites to bind metal ions. The polymer-anchored reagents or ligands then react with suitable metal precursors to give the polymer-anchored complexes [24]. Sherrington has developed wide range of polymer-supported metal complexes as catalysts and used them for various catalytic reactions [18].

Carboxylic acid and sulfonic acid functions may react with -CH₂Cl in mild basic conditions. N(CH₂CH₃)₃ in ethylacetate was often used to abstract the HCl produced in the reaction (Scheme 2) [25–27]. In many cases the reaction is carried out at 90 °C for effective anchoring. During this process the -COOH group of e.g. 3-formylsalicylic acid reacts with the -CH₂Cl group of polystyrene. Covalent bonding through the -COOH group of ligands has also been demonstrated by reacting benzylchloride with ligands e.g. H₂fsal-ea and H₂fsal-ohyba, under similar reaction conditions. Phenolic hydroxyl group requires alkali carbonate along with N(CH₂CH₃)₃.

Some of the polymer-anchored ligands synthesized by this method are presented in Scheme 3 [26–32]. Porphyrins such as 5,10,15-tris(4-R-phenyl)-20-(4-hydroxyphenyl)porphyrin bearing peripheral hydroxyl group have been covalently linked to PS-CH₂-Cl (XIV of Scheme 3) by carrying out the reaction in DMF at 80 °C in the presence of K₂CO₃ [33].

The synthesis of the polymer-anchored ligand, PS-H₂fsal-β-ala (XV) was achieved in two steps [34] as represented in Scheme 4.

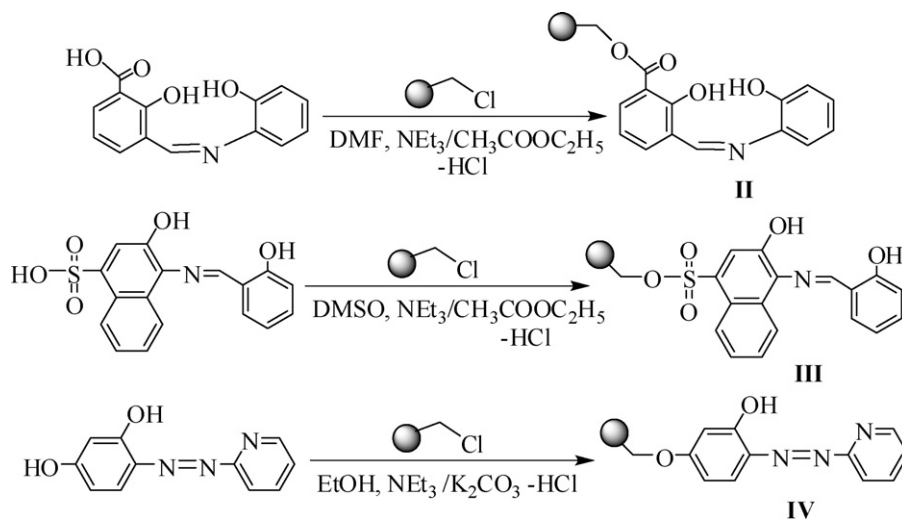
Other ligands XVI and XVII (Scheme 5) were prepared similarly [35].

On reaction with 1,2-diaminocyclohexane the polymer-bound salicylaldehyde gives the mono condensed ligand leaving one amino group free. Further reaction of this compound with di-*tert*-butylsalicylaldehyde gives the chiral “non-symmetrical” polymer-anchored dibasic tetradentate ligand XVIII (Scheme 6) [36].

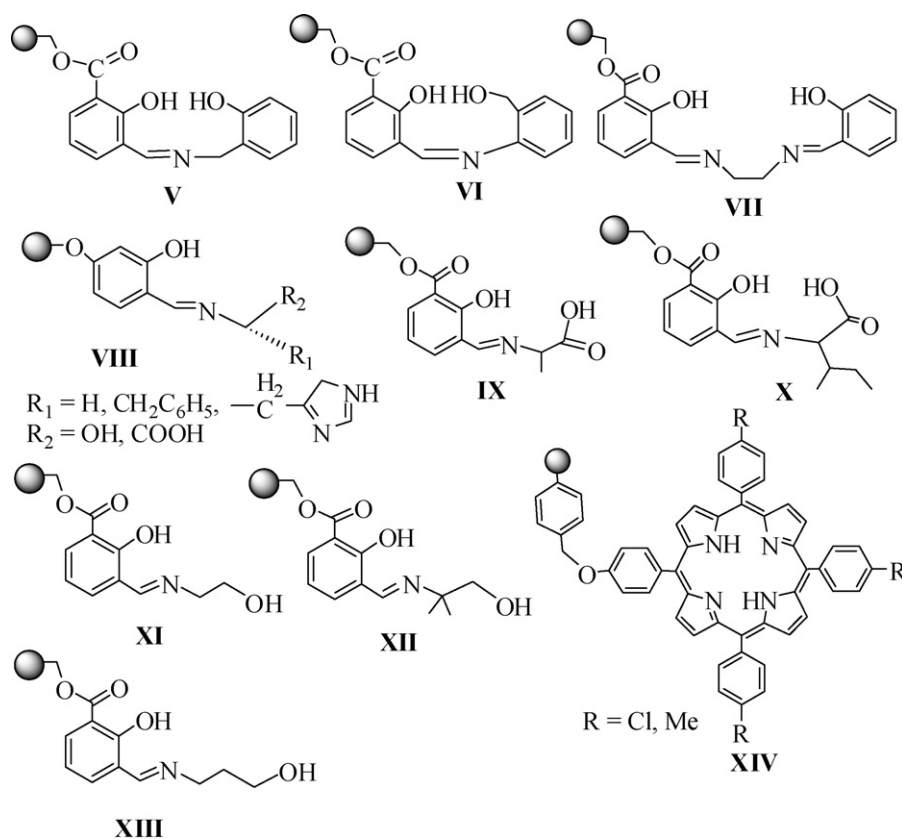
PS-CH₂-Cl also reacts with the -NH included in rings of e.g. imidazole under the reaction conditions prescribed for the carboxylic acid group to give the polymer-anchored ligand. Thus, reaction between PS-MeCl and Hhpbmz in DMF in the presence of triethylamine lead to the formation of polymer-anchored PS-Hhpbmz ligand (Scheme 7) [37]. Miller and Sherrington reported that 2-(2-pyridyl)imidazole can be similarly anchored onto polystyrene, through covalent attachment of imine nitrogen, by the reaction of ligand and PS-MeCl in refluxing toluene [38].

Under above reaction conditions, PS-MeCl was also shown to react with 2-pybmz and 3-pybmz, and even H₂salten in DMF to give the polymer-anchored PS-2-pybmz (XX), PS-3-pybmz (XXI) [39] and PS-H₂salten (XXII), respectively (Scheme 8) [40].

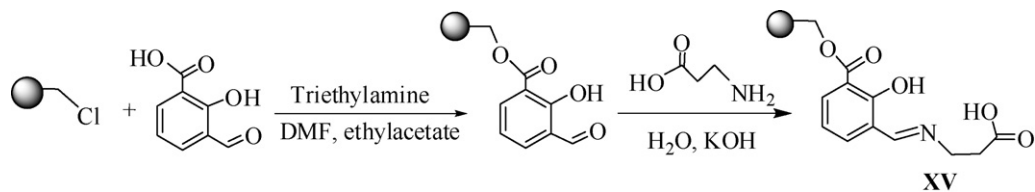
These polymer-anchored dibasic tetradentate and dibasic tri-dentate ligands, on reaction with [V^{IV}O(acac)₂] (in DMF) or



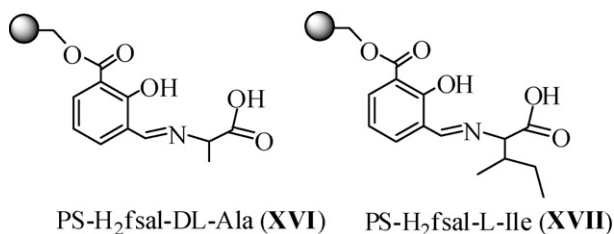
Scheme 2. Examples of reactions to establish covalent bonds between ligands and PS-CH₂Cl. The ball represents the backbone of chloromethylated polystyrene.



Scheme 3. Structural formula of several prepared polymer-anchored ligands.



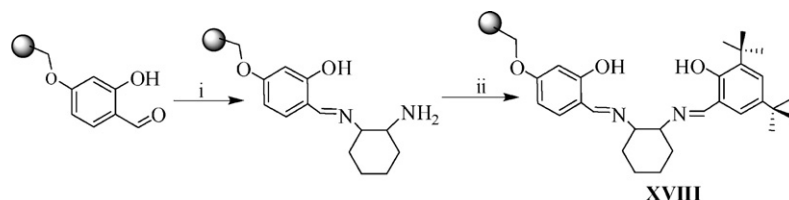
Scheme 4. Reaction scheme for the synthesis of PS-H₂fsal-β-Ala (XV).



Scheme 5. Suggested Structural formulas of **XVI** and **XVII**.

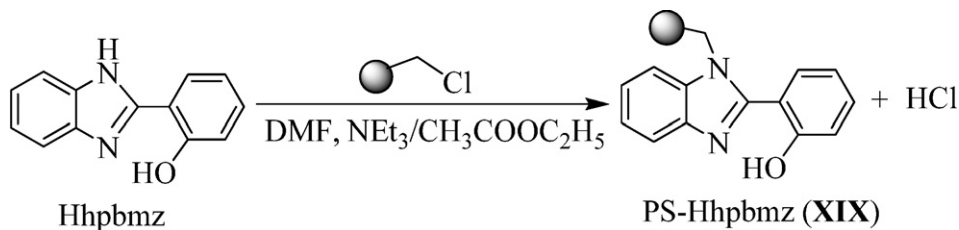
V^{IV}OSO₄ (in methanol/water), gave the corresponding oxido vanadium(IV) complexes. Some of the complexes isolated are grouped in [Scheme 9](#).

On aerial oxidation of PS-[V^{IV}O(fsal-ohyba)(DMF)] (**1**) in the presence of KOH in DMF, the V^VO₂-complex PS-K[V^VO₂(fsal-ohyba)] (**2**) was obtained. Similarly, addition of H₂O₂ to PS-[V^{IV}O(fsal-ohyba)(DMF)] suspended in acetonitrile in the presence of KOH gave PS-K[V^VO(O₂)(fsal-ohyba)] (**3**) ([Scheme 9](#)). The change of the color of the resin particles could also be visualized during the reactions [\[30\]](#). The V^VO₂-complex PS-K[V^VO₂(fsal-ohyba)] (**2**) could also be obtained by the reaction of

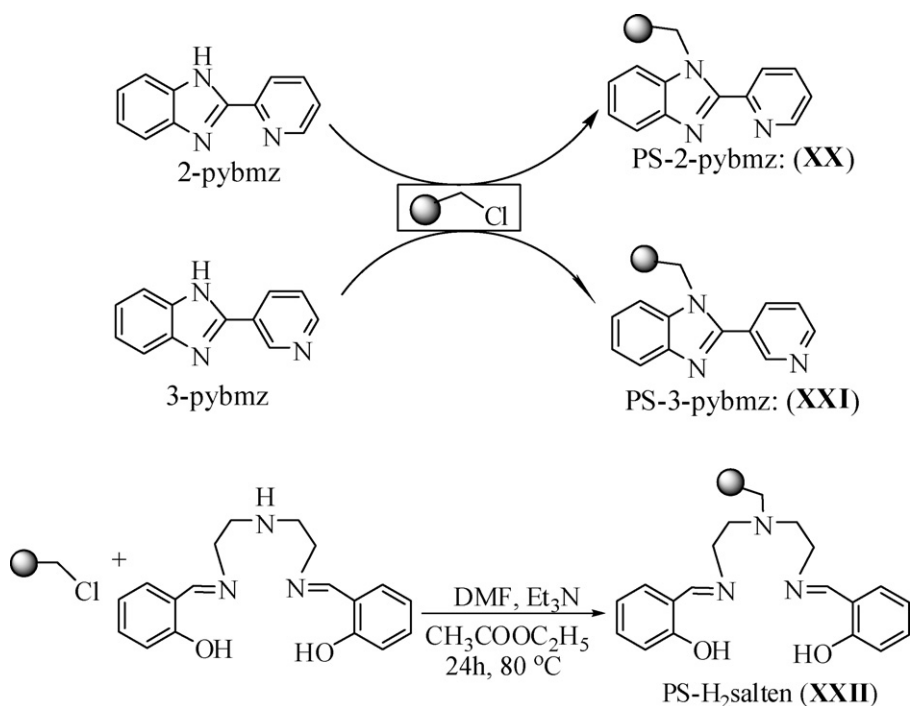


- (i) (S,S)-1, 2-diaminocyclohexane, dioxane, 18-Crown-6, K₂CO₃, 85 °C, 3 days.
 (ii) Salicylaldehyde derivatives, 18-Crown-6, K₂CO₃, 85 °C, 3 days.

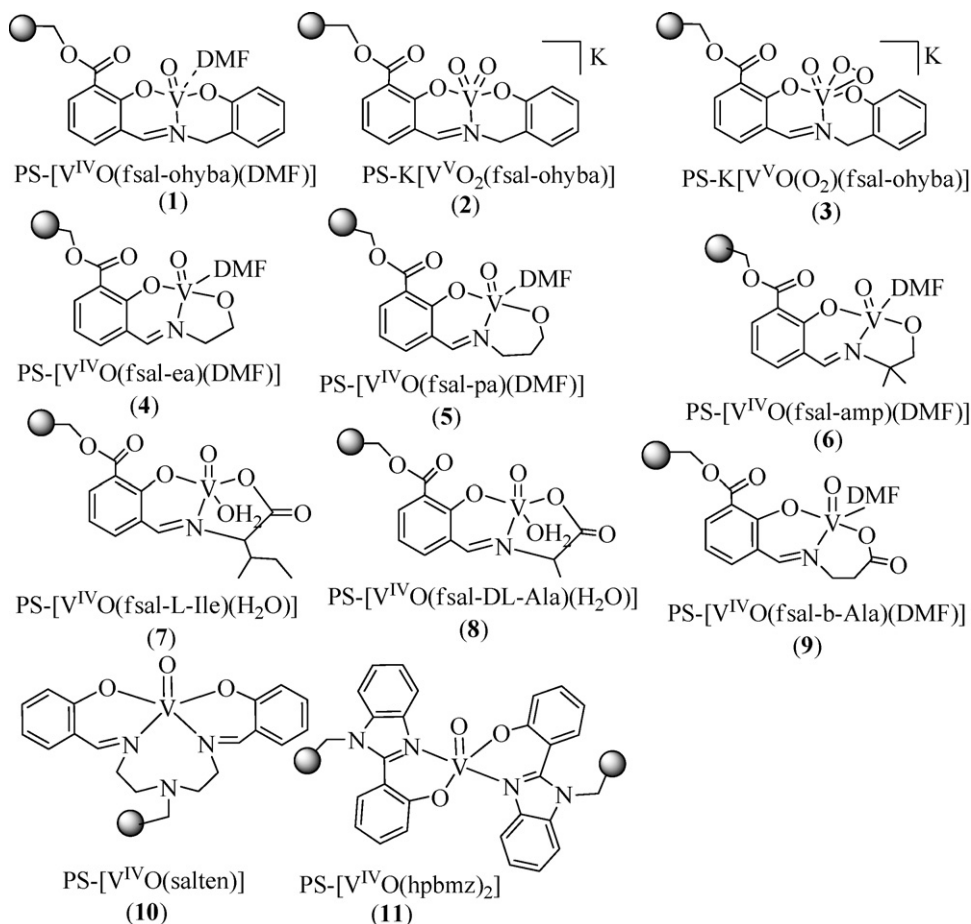
Scheme 6. Synthesis of anchored salen-type ligands [\[36\]](#).



Scheme 7. Preparation of PS-Hhpbmz (**XIX**).

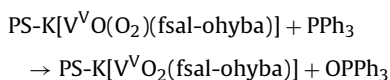


Scheme 8. Preparation of **XX**, **XXI** and **XXII**.



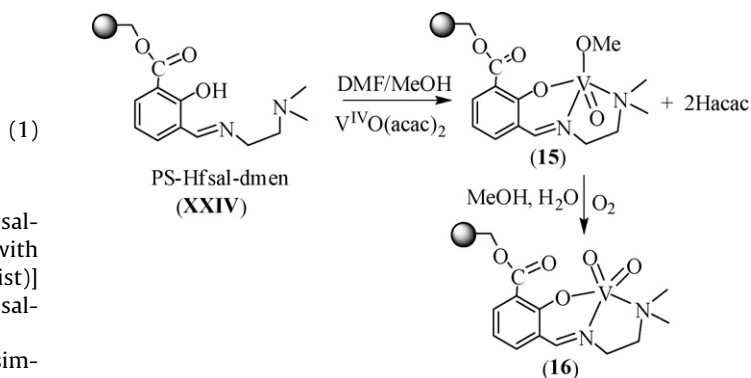
Scheme 9. Suggested structural formulas of several of the prepared polystyrene bound complexes discussed in this work. The ball represents the polymer matrix.

PS-K[V^VO(O₂)(fsal-ohyba)] (**3**) with PPh₃, Eq. (1).

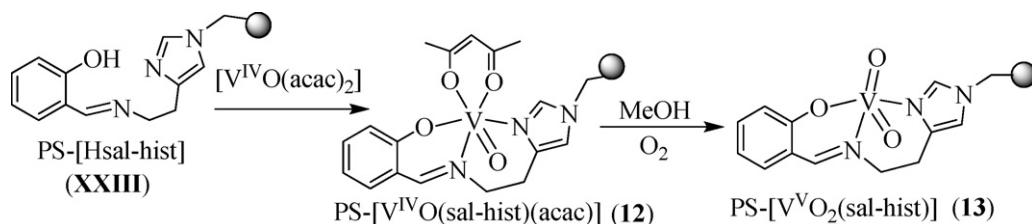


Immobilization of [V^{IV}O(sal-hist)(acac)] to give PS-[V^{IV}O(sal-hist)(acac)] (**12**) involved the reaction of PS-Hsal-hist (**XXIII**) with [V^{IV}O(acac)₂] in DMF. Aerial oxidation of PS-[V^{IV}O(acac)(sal-hist)] in methanol gave the dioxovanadium(V) complex PS-[V^VO₂(sal-hist)] (**13**) (Scheme 10) [41].

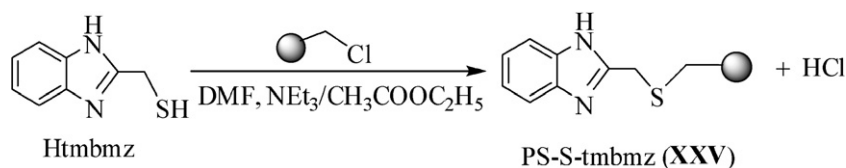
Complex PS-[V^{IV}O(fsal-aepy)(acac)] (**14**) was prepared similarly. However, ligand PS-Hfsal-dmen (**XXIV**) under similar conditions gave PS-[V^{IV}O(fsal-dmen)(OMe)] (**15**) which on oxidation gave the expected V^VO₂-complex, PS-[V^VO₂(fsal-dmen)] (**16**) (Scheme 11). The presence of MeO[−] in PS-[V^{IV}O(fsal-dmen)(OMe)] was confirmed by GC–MS upon keeping it in DMSO for ca. 15 h and detecting MeOH in liquid part of the mixture [42].



Scheme 11. Formation of PS-Hfsal-dmen (**XXIV**), PS-[V^{IV}O(fsal-dmen)(OMe)] (**15**) and PS-[V^VO₂(fsal-dmen)] (**16**) [42].



Scheme 10. Scheme for the synthesis of polymer supported complexes [41].



Scheme 12. Reaction of Htmbmz with PS-MeCl [43].

The reaction of Htmbmz with the PS-CH₂- fragment yielded a product designated as PS-ligand, which corresponds mostly to the tmbmz bound to the polystyrene matrix by the sulfur atom (Scheme 12). Although the product formed in the reaction of Htmbmz with benzyl chloride, where the sulfur atom acts as the nucleophile in the reaction, confirms the condensation of Htmbmz with benzyl chloride, the reaction of PS-MeCl with Htmbmz did not yield clean PS-S-tmbmz (XXV), according to Scheme 12. The analytical results obtained, namely the S/N ratio, did not fully agree with the formation of XXV, and products corresponding to a higher relative % of sulfur also form. It is possible that, before and after the Htmbmz binds to the solid, the thiol group oxidizes to disulfide, other oxidation products possibly also forming, and these are discussed in the original publication made [43]. As the exact nature of the complexes obtained from XXV is not known, these were designated by PS-[V^{IV}O(ligand)_n] (17).

Metal complexes as such may form covalent bonds if a suitable coordinating site is present on the functional group attached to polymer. Thus, reaction of imidazolomethylpolystyrene (PS-im) with dioxovanadium(V) complexes K[V^{VO}O₂(sal-inh)]·H₂O and K[V^{VO}O₂(sal-bhz)]·H₂O dissolved in DMF gave the imidazolomethylpolystyrene bound complexes PS-K[V^{VO}O₂(sal-inh)(im)] (18) and PS-K[V^{VO}O₂(sal-bhz)(im)] (19), respectively (Scheme 13) [44]. The energy dispersive X-ray (EDX) analyses supported the presence of 1.2% and 1.0% vanadium in PS-K[V^{VO}O₂(sal-inh)(im)] and PS-K[V^{VO}O₂(sal-bhz)(im)], respectively.

2.2. Encapsulation of vanadium complexes in zeolite-NaY

Zeolites are crystalline hydrated aluminosilicates with open framework structures constructed from AlO₄ and SiO₄ tetrahedra linked to each other by sharing all oxygen atoms, forming nanocavities and nanochannels of strictly regular dimensions and of different sizes and shapes. A large variety of zeolites may be obtained, depending on the conditions used during their synthesis. Zeolite crystals are porous on a molecular scale and

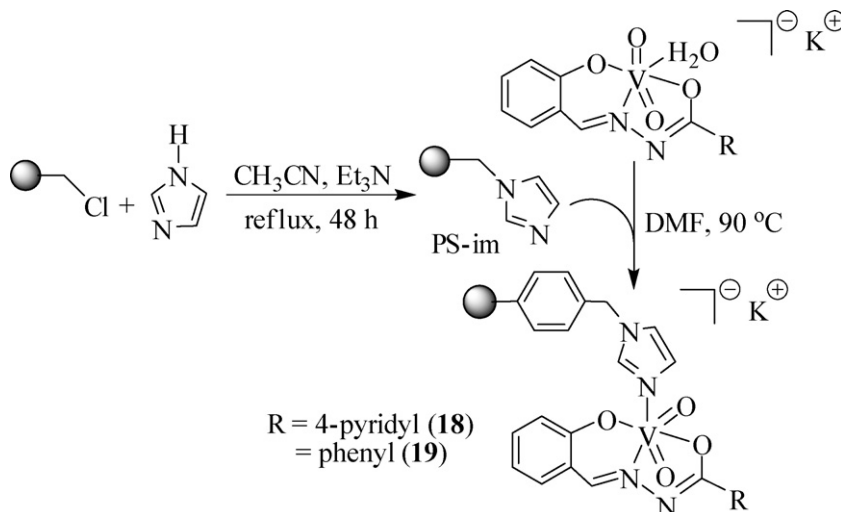
their framework contains regular arrays of channels and cavities. In particular, the structure of zeolite-Y consists of almost spherical 1.3 nm cavities interconnected tetrahedrally through smaller apertures of 0.74 nm diameters [45] which are occupied by exchangeable cations and water molecules. The exchangeable properties of extra-framework cations and the suitable cavity size of the zeolites allow their modification by inclusion of adequate molecules, namely homogeneous catalysts (i.e. metal complex), and hence the term zeolite-encapsulated metal complexes. The large size of the encapsulated homogeneous catalysts and their rigidity make them difficult to escape out of the zeolite cages (Scheme 14).

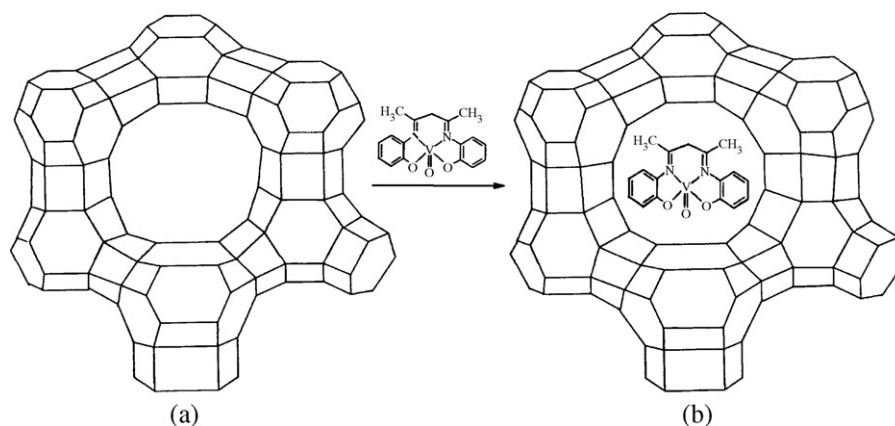
The encapsulation of V^{IV}O-complexes was often used to modify the original properties of porous catalyst hosts in nanoporous structures, namely of zeolite-Y. Both the acidity and redox properties can be modified by inserting V^{IV}O-complexes into the supercage of the zeolite.

Normally, three general approaches to the preparation of zeolite-encapsulated metal complexes are considered: (i) flexible ligand method (FL), (ii) template synthesis method (TS) and (iii) zeolite synthesis method. In addition to these, other two approaches: ion exchange and adsorption methods have also been applied. These methods are briefly discussed below [46,47].

Encapsulation of vanadium complexes in the nanocavities of zeolite-Y has been carried out by the FL method where the ligand is flexible enough to pass through the restricting zeolite pores and get into the larger cavities and reacts with previously exchanged V^{IV}O²⁺ ions. The resulting complexes are larger and more rigid entities, and do not escape from the nanocavities. The purification of crude masses by Soxhlet extraction removes the excess of free ligand and along with the neat complex formed on the external surface of the support. The non-complexed V^{IV}O²⁺ ions remaining, if any, are removed by exchanging back with aqueous 0.01 M NaCl solutions.

If the metal complex is formed in a limited number of reaction steps, assembly of the ligand from small species within the pores may be preferred. Assembling ligands from smaller species inside

Scheme 13. Formation of PS-K[V^{VO}O₂(sal-inh)(im)] (18) and PS-K[V^{VO}O₂(sal-bhz)(im)] (19) [44].



Scheme 14. Structure of zeolite-Y (a) and metal complex encapsulated in zeolite-Y (b).

the nanopores corresponds to the template synthesis method (TS). Normally, the $V^{IV}O^{2+}$ ions are introduced into the nanopores by ion exchange, or by pre-adsorption followed by reaction of the smaller molecular fragments with the metal ions to form the desired metal complex within the pores [48].

In some cases, namely when the metal complexes are able to withstand the conditions of the synthesis of the support and sufficiently soluble in the synthesis medium to enable random distribution of the complexes in the synthesized porous materials, the synthesis of the molecular sieve structure may be done around the preformed complex, this being designated as zeolite synthesis method, or sol–gel synthesis method.

Inside the zeolite cages the metal complex should be free to move about within the confined volume of the cavities, but is prevented from leaching by the size of the pore openings. Hence, the application of the term zeolite ship-in-a-bottle (SB) complex has been used for such complexes. It can be anticipated that metal complexes not bound to the zeolite surface will retain solution-like activity; however, the crystalline microporous host is also expected to impart size and shape selectivity to the catalyst. Additionally, the zeolite may also provide a stabilizing effect since multimolecular

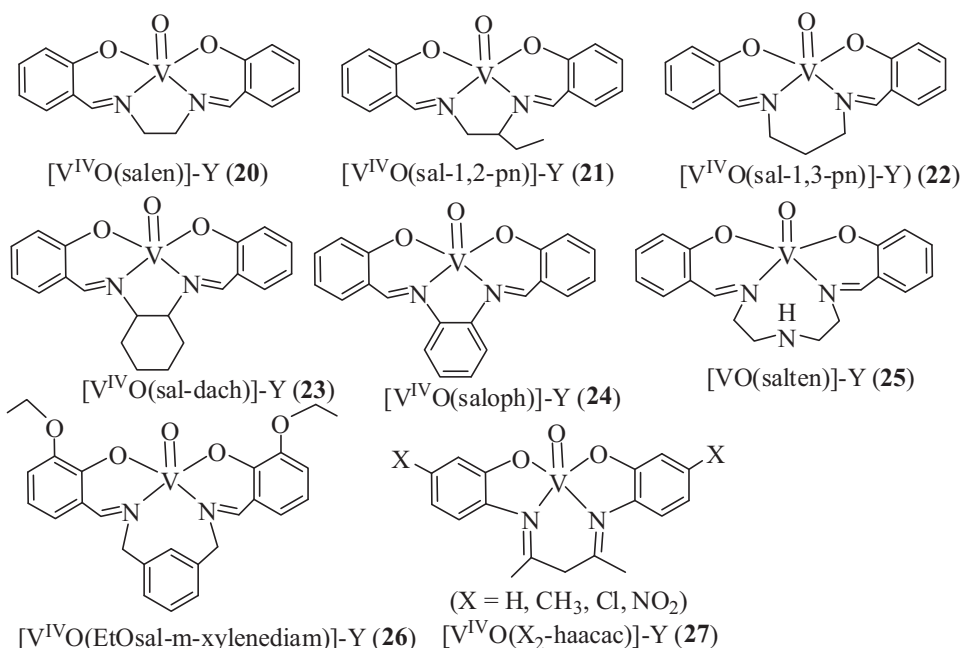
deactivation pathways such as formation of μ -oxido or -peroxido bridged species will be precluded.

Aerial oxidation of the encapsulated $V^{IV}O$ -complexes in solvent may convert them to V^VO - or V^VO_2 -complexes, depending on their oxygen demand and coordination requirement. Schemes 15 and 16 present examples of zeolite encapsulated complexes (20–32) prepared by this method [48–59].

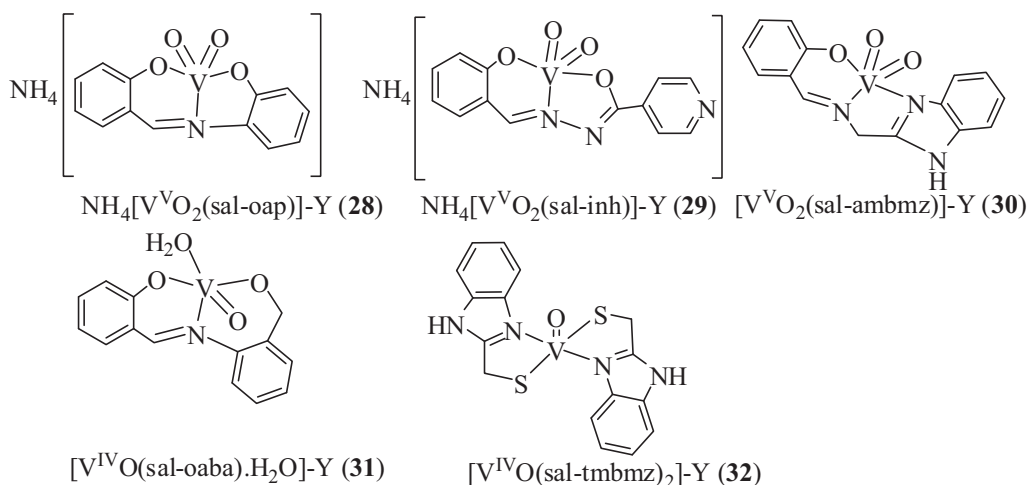
Encapsulation of e.g. vanadium phthalocyanine complex in zeolite-Y [$V^{IV}Pc$]-Y (33) was achieved by the “template synthesis method” where the phthalocyanine was prepared using precursors in the presence of zeolite-Y followed by its reaction with $V^{IV}OSO_4$ [60].

$V^{IV}O$ -tetraaza complexes of [14]ane N_4 and [16]ane N_4 encapsulated in the nanopores of zeolite-Y were also prepared by in situ condensation of ethylcinnamate with the corresponding previously encapsulated [$V^{IV}O$ (bis-diamine) $_2$] $^{2+}$ -complexes: [$V^{IV}O$ (N-N) $_2$] $^{2+}$ -Y (Scheme 17) [61].

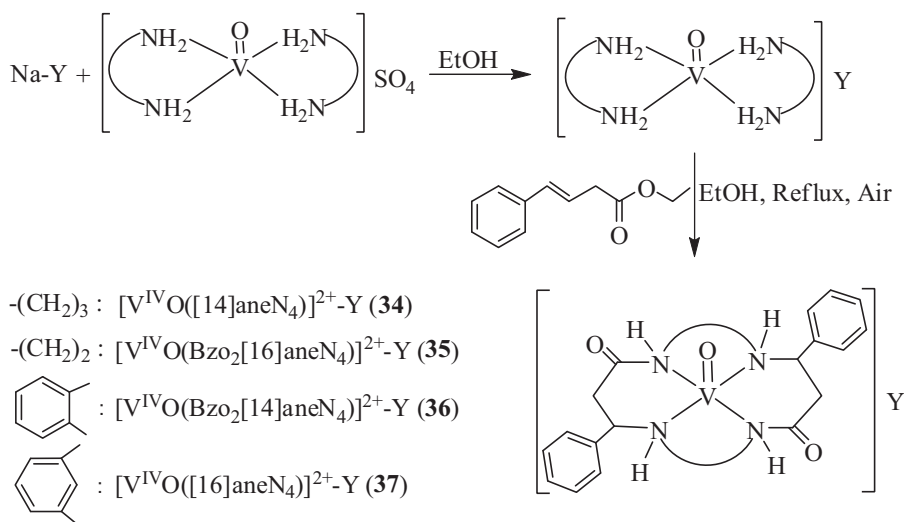
Using a similar approach, the [$V^{IV}O$ ([R] $_2$ -N $_2$ X $_2$)] $^{2+}$ -Y (R = H, CH $_3$, X = NH, O, S) complexes were entrapped in the nanocavity of zeolite-Y. Here, adsorption of the precursor ligand 1,2-di(o-aminophenyl-, amino, oxo, thio)ethane, (N $_2$ X $_2$) first took place in



Scheme 15. Proposed structural formulas of zeolite-Y encapsulated complexes 20–27.



Scheme 16. Proposed structural formulas of zeolite-Y encapsulated complexes 29–32.

Scheme 17. Synthesis of zeolite-Y encapsulated V^{IVO} -tetraaza complexes [61].

the supercages of V^{VO} -Y to give $([\text{V}^{\text{IVO}}(\text{N}_2\text{X}_2)]^{2+}\text{-Y})$ ($\text{X}=\text{NH}, \text{O}, \text{S}$) which upon condensation with glyoxal or biacetyl gave $[\text{V}^{\text{IVO}}(\text{R})_2\text{-N}_2\text{X}_2]^{2+}\text{-Y}$ ($\text{R}=\text{H}, \text{CH}_3$) (Scheme 18) [45].

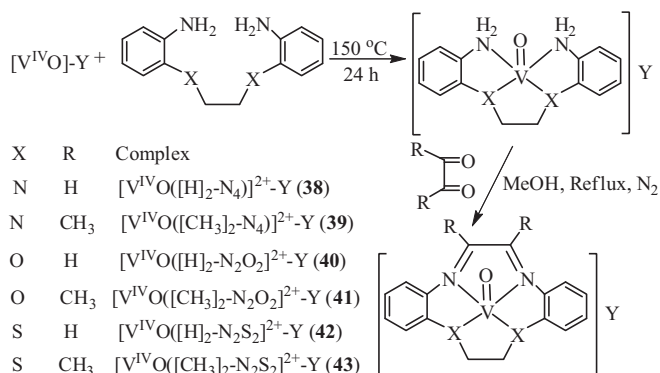
V^{IVO} -exchanged faujasite ($\text{V}^{\text{IVO}}\text{O}^{2+}\text{-Y}$) allows bipyridine complexation, giving a heterogeneous “ship-in-a-bottle” catalyst denoted as $[\text{V}^{\text{IVO}}(\text{bpy})_2]^{2+}\text{-Y}$ (44). These cationic complexes are intrazeolitic and homogeneously distributed across the zeolite

crystals and both the zeolite and the neutral bipyridine ligands stabilize V^{IV} [62].

2.3. Immobilization of vanadium complexes on ordered mesoporous silicas

Due to the size restrictions in zeolite-Y, the encapsulation of large complexes is difficult. In fact, as it imposes some geometrical restrictions on the complexes to accommodate them, it may be difficult for substrates to diffuse in and access the active sites, and for products to diffuse out of the pores. Hence the focus has been shifting to mesoporous materials having larger pores and higher surface area. Since direct encapsulation of such complexes in mesoporous supports may not be advantageous due to their leaching in the presence of solvents, the binding of these metal complexes to the support is preferred. Additionally the mesoporous materials have attracted much attention because of their mechanical stability, well-ordered pore arrays, large specific surface area, uniform pore size distributions and tunable pore diameter (4–15 nm), and MCM-41 and SBA-15 have been the most frequently used mesoporous materials for the immobilization of homogeneous chiral catalysts [21].

For many applications, particularly for enantioselective synthesis, it is necessary to protect free surface silanol groups, to have a

Scheme 18. Synthesis of entrapped zeolite-Y V^{IVO} -complexes 38–43 [45].

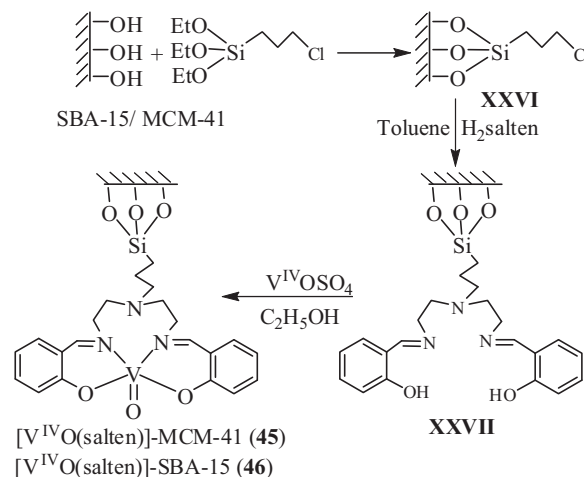
linker of sufficient length, and to choose the appropriate solvent [21,63]. In this way, the complex may behave like that in homogeneous phase, but still anchored to the solid surface. Indeed, the catalysts are truly heterogeneous and retain a significant percentage of their initial activity and enantioselectivity. In some cases the tether linking (organic spacer) between the complex and the solid surface should be long enough to permit the complex to have a large conformational freedom and the solid surface must be modified to reduce the presence of residual silanol groups. In other cases, probably due to confinement and shape selectivity effects, the final selectivity or enantioselectivity may be significantly increased compared with the homogeneous catalyst.

Due to the existence of hydroxyl groups on the surface of the mesoporous molecular sieves MCM-41, SBA-15 and Hexagonal mesoporous silica (HMS), the immobilization of metal complexes is mostly achieved by first functionalizing them with adequate organic spacers, followed by covalent anchoring (post-grafting method) of the ligand or metal complexes to the functionalized mesoporous materials. Functionalization of the mesoporous materials may be achieved by e.g. silanation of the mesoporous surface with 3-amino- or 3-halogenopropylalkoxysilanes in a polar solvent.

Some catalysts are grafted inevitably on the external surface of the supports. However, the external surface area of the support is much less than that contributed by the nanopores of the support and additionally there are also processes to passivate the external SiOH groups [21]. Several review articles give accounts on these subjects [11–13,17,21,20] and provide detailed accounts of such immobilized complexes [13].

Joseph and Halligudi have reported the anchoring of $[V^{IV}O(\text{salen})]$ on SBA-15 [64] and MCM-41 [65] by functionalizing it using the above outlined methodology as shown in Scheme 19. Parida et al. [66] have also grafted $[V^{IV}O(\text{salen})]$ on MCM-41 using a similar method. Again it was observed that the mesostructure was not destroyed during the multi-step synthetic procedures used.

Mesoporous silica MCM-41 was also organofunctionalized by 3-aminopropyltrimethoxysilane (APTS) on the surface of its nanochannels. The amino groups on the solid were then used to coordinate to the $V^{IV}O^{2+}$ ions (Scheme 20). Immobilization of the



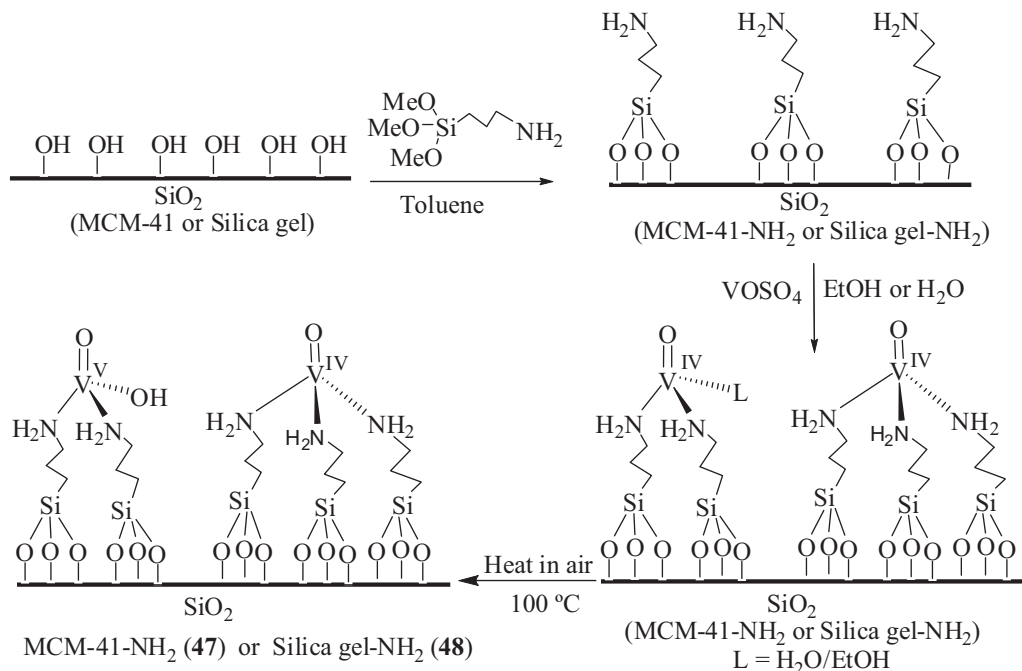
Scheme 19. Grafting of $[V^{IV}O(\text{salen})]$ on MCM-41 and SBA-15 by first binding an organic spacer, then anchoring the ligand and finally introducing the metal ion [64,65].

metal ion on functionalized surface has the advantages of better control of available reactive sites and site isolation [67].

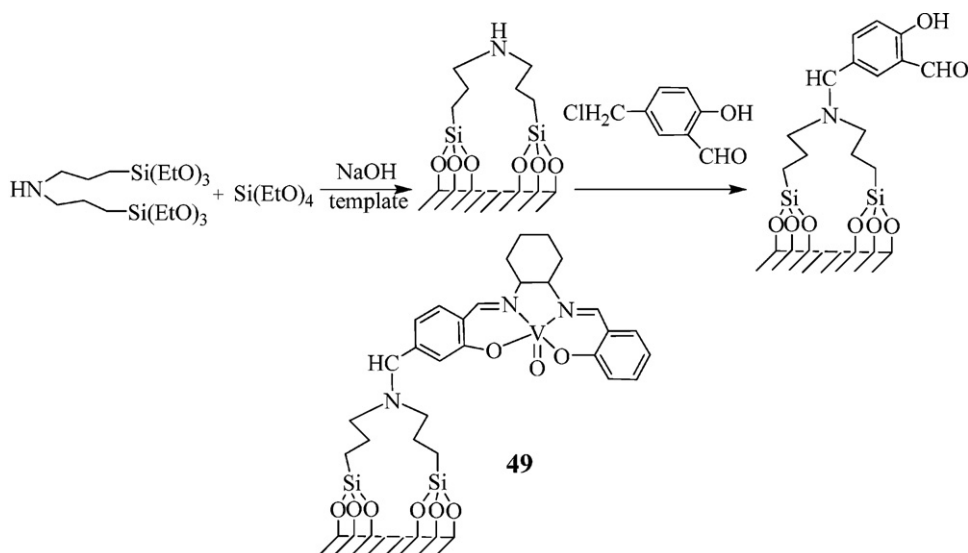
A secondary amino group modified MCM-41 was synthesized and used as a support for the immobilization of $[V^{IV}O(\text{salen})]$ also via a multi-grafting method (Scheme 21) [68].

Other $V^{IV}O$ -Schiff base complexes having a terminal carbon-carbon double bond at alkyl chains of various lengths attached to the *para* position of the salen-type ligand were anchored on several supports including MCM-41, after inserting a spacer with mercaptopropylsilyl groups as shown in Scheme 22 [69].

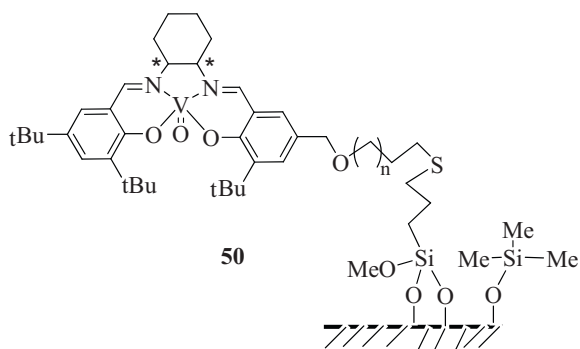
These grafting strategies were applied to immobilize $[V^{IV}O(\text{acac})(\text{Ph-DAB}-(\text{CH}_2)_3\text{Si}(\text{OEt})_3)\text{Cl}]$ on MCM-41 (**52** of Scheme 23(A)). Here, the $V^{IV}O$ -complex bound to two triethoxysilyl groups present on 1,4-diazabutadiene (DAB) was reacted with MCM-41 in toluene/methanol in the presence of a small amount of HCl to yield the complexes on MCM-41 [63]. A very similar method was applied (Scheme 23(B)) to prepare complex **53** [70].



Scheme 20. Binding of $V^{IV}O^{2+}$ to MCM-41-NH₂ and silica gel-NH₂.



Scheme 21. The upper part shows schematically the modification on MCM-41 with a secondary amine and binding of a salicylaldehyde derivative. The lower section shows the final complex **49** attached to the modified MCM-41.



Scheme 22. The MCM-41 complex **50**, with the deactivated SiOH groups [69]. The ligand contains two stereogenic carbon atoms.

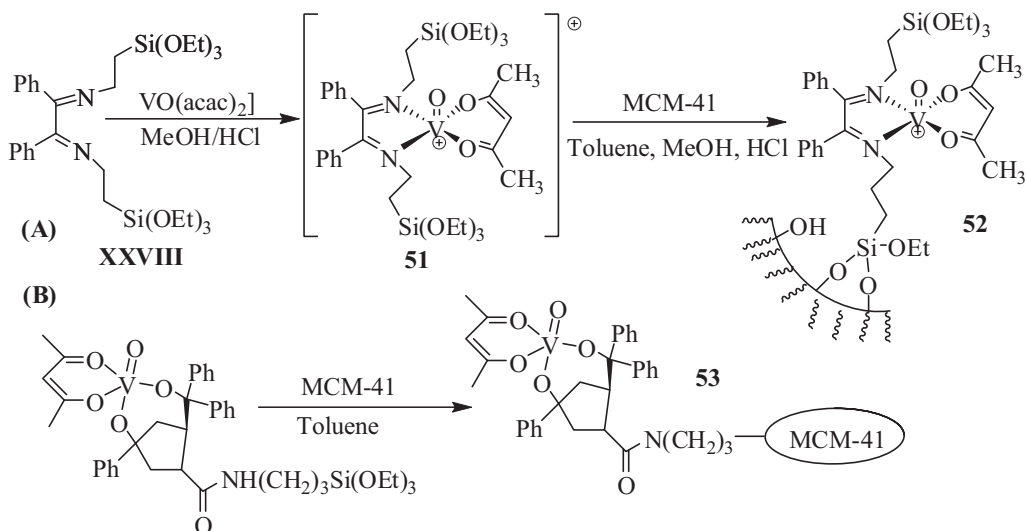
Hexagonal mesoporous silicas (HMS) are also ordered mesoporous materials having hydroxyl groups at their surface. Immobilization of $[V^{IV}O(acac)_2]$ onto a synthetic HMS using three different methodologies was reported. In first method,

$[V^{IV}O(acac)_2]$ was directly immobilized onto the parent material; the second method involves the functionalization of HMS with 3-aminopropyltriethoxysilane (APES) followed by covalent complex grafting. The third method is similar to the second one but in presence of trimethylsilane to deactivate the silanol groups and subsequent complex grafting [71–73]. Several other solid matrices, namely alumina, silica gel, mesoporous silicas, polystyrene and clays [74–78] were used to immobilize $[VO(acac)_2]$. It was also immobilized by covalent grafting onto amine functionalized activated carbon [79].

3. Characterization methods

3.1. Analytical data

There are several methods for the characterization of heterogenized complexes and the choice of the set of methods to use depends on the particular case in hand, namely if the support is a polymer such as polystyrene, or a Si-based support such as



Scheme 23. (A): Preparation of $\{[V^{IV}O(acac)(Ph-DAB-(CH_2)_3Si(OEt)_3)Cl]\}$ -MCM-41 [63]. (B): Preparation of $\{V(O)(acac)[(2S,4R)-N-(3-triethoxysilyl)propylaminocarbonyl-4-hydroxy-4-phenyl-2-(1,1-diphenylmethyl)pyrrolidinylmethanol]\}$ -MCM-41 [70].

zeolite-NaY or MCM-41, if the metal centre is paramagnetic i.e. a V^{IV} -complex, or if it is diamagnetic i.e. a V^V -complex, etc.

The complexation of a vanadium species with bound ligands is frequently accompanied by color changes of the solid support, namely if it is a V^{IV} O-complex. This is already an indication that the catalyst may in fact be bound to the support. Whatever the nature of the solid support or complex, the determination of the elemental analysis is one of the important steps to characterize the supported catalyst.

For polystyrene-bound complexes, the analytical results for metal content, as well as for N and S (if present) are relevant. The simple existence of a non-zero %V or %N is a clear indication of the binding of the complex to the PS-matrix. If the ratio of %V:%N is close to those of the neat complex, this is a good indication that the anchored compound has a similar nature. The V loading in the catalyst (and in the leaching solution) may be determined by atomic absorption spectroscopy (AAS) or using an inductively coupled plasma (ICP) spectrometer after adequate treatment of the catalyst. The residue obtained at the end of a thermogravimetric analysis (TGA) may also afford the V loading in the catalyst.

In the case of zeolite-Y or MCMs, the Si content may be obtained gravimetrically as SiO_2 . The Si/Al molar ratio of zeolite-Y is ca. 2.5 and upon heterogenization of the complexes is not expected to change. The binding of $V^{IV}O^{2+}$ to zeolite-Y is accompanied by a color change to light blue and by a decrease in the %Na. The subsequent binding of a ligand may yield further color changes e.g. to pale blue–green. Either for zeolite-Y or for e.g. MCM-41, the simple existence of a non-zero %V, %C or %N (or %S, if present) is a clear indication of the binding of the complex to zeolite-Y. If the ratio of %V:%C:%N is close to these ratios in the neat complex, this is a good indication that the anchored compound has a similar nature.

The vanadium content of the solids per weight may be similar when comparing zeolite and MCMs, or several different MCMs, but the vanadium content per surface area is also a parameter to take into account. The density of complexes per surface area may differ considerably and has relevance for the catalytic activity [70].

3.2. IR and Raman spectroscopy

IR and Raman spectroscopy are very important techniques for the characterization of heterogenized complexes, and has even been considered to be the best solid-state technique to indicate encapsulation in host–guest supramolecular structures [80].

IR and Raman spectroscopy has been useful to characterize polystyrene-bound ligands and their complexes. The PS-MeCl exhibits strong peaks at 1264 and 673 cm^{-1} due to the CH_2Cl group. Upon the covalent bonding of PS-MeCl to ligands, these bands normally disappear [81]. Bands of medium intensity appear at 2800–2990 cm^{-1} due to the presence of CH_2 group of polystyrene. In ligands and complexes attached through carboxylic groups to the polymer, the appearance of a sharp band at ca. 1670 cm^{-1} due to $\nu(C=O)$ of carboxylate may confirm their binding [75]. The covalent bonding of benzimidazole ligands through the N-atom of the ring is reflected by the disappearance of the broad features of the NH stretching band at 2650–2800 cm^{-1} . Comparison of spectral patterns of neat with polymer-supported ligands as well as complexes may also provide useful information to confirm the establishment of bonds between the ligand and metal ion in complexes. For example, $\nu(C=N)$ (ring) in PS-tmbmz, PS-Hhebzmz, PS-Hhpbmz, PS-2-pybmz and PS-3-pybmz shifts to lower wave numbers in the corresponding polymer-anchored complexes [37,39,82,83]. Other ligands may exhibit characteristic $\nu(C=N)$ (azomethine) bands which shift to lower wave numbers (or higher) in complexes. In addition the $V^{IV}O$ -complexes normally display a sharp band at ca. 950–990 cm^{-1} while V^VO_2 -complexes exhibit two such bands at slightly lower energy, ca. 950–870 cm^{-1} . The peroxo complex PS-

$K[V^VO(O_2)(fsal-ohyba)]$ showed three IR active modes associated with the $\{V(O_2)\}^{2+}$ moiety, namely the symmetric $V(O_2)$ stretch at 591 cm^{-1} , the antisymmetric $V(O_2)$ at 773 cm^{-1} , and the O–O stretch at 860 cm^{-1} , characteristic of η^2 -coordination of the peroxo group [30].

In zeolites and mesoporous MCM-41 materials the $\nu_s(Si-O)$ siloxane appear in the range 770–850 cm^{-1} , a $\delta(Si-O)$ mode of the Si–OH appears at ca. 965 cm^{-1} , $\nu_{as}(Si-O)$ and $\nu_{as}(Al-O)$ at ca. 1130 cm^{-1} [52] and isolated silanol (Si–OH) vibrational bands at ca. 3750 cm^{-1} [20,84]. The ν_{as} modes of the Si–O–Si vibration appear at ca. 1235 and 1060–1090 cm^{-1} and the ν_{sym} mode at ca. 790–820 cm^{-1} [20]. Often a band at ca. 1630 cm^{-1} and a broad band at ca. 3450 cm^{-1} is also observed in the spectra and is attributed to H–O–H bending vibrations of physisorbed water. The degree of silylation in the solid materials may be determined by comparing the area of the OH stretching bands in the IR for each solid before and after silylation. To avoid the interference of co-adsorbed water in the measurements of the silanol group population, before recording the IR the solids should be degassed at ca. 100 °C under reduced pressure for ca. 1 h [69].

IR spectroscopy can provide valuable information on the integrity of the encapsulated complexes as well as on the crystallinity of the host zeolite. Peaks due to the zeolite-NaY normally dominate the spectra and some of the major zeolite framework bands appear around 1140, 1040, 960, 785 and 740 cm^{-1} [52]. The intensity of IR bands of heterogenized complexes depends on their loading, but normally it is weak due to their low concentration in the zeolite [45,48,50,51,61,85].

The anchoring of ligands to the support may be confirmed by the appearance of characteristic bands e.g. 1620–1690 cm^{-1} ($C=N$), 1450–1560 cm^{-1} (aromatic $C=C$), ca. 1500–1550 cm^{-1} (aromatic $CH-$), 1550–1610 and 1350–1420 cm^{-1} ($C=O$) and 1280–1290 ($C-O$) [50,51,65]. Often these bands undergo only marginal shifts in positions upon immobilization of the ligands or complexes by encapsulation. Upon grafting of the ligand the shifts observed depend on the position of the IR active group but often the changes are not very pronounced. The $V^{IV}O$ has a characteristic $\nu(V=O)$ at 950–990 cm^{-1} , but in many cases it cannot be located in zeolite-Y supports due to the appearance of a strong and broad band of the zeolite framework in the 1390–900 cm^{-1} region [45,48,61].

While the observation of shifts in bands of $VO(L)$ complexes, or even the fact that they are not observed because they are hidden by the framework bands of the solids may be indicative of encapsulation or anchoring of $VO(L)$ complexes, the observation, as mentioned for one sample of zeolite- $V^{IV}O(Salen)-Y$, that the spectrum is just the simple sum of the spectrum of $V^{IV}O(Salen)$ and that of zeolite-Y, was considered as proof that in this particular sample the complex is only superficially impregnated on zeolite-NaY [85].

Raman spectrum of zeolite-Y shows only an intense band at 500 cm^{-1} that can be assigned to a bending vibration of Si–O–Si. Two other low-intensity bands near 800 cm^{-1} and 1100 cm^{-1} were assigned as symmetric and asymmetric stretching modes $\nu_s(SiO)$ and $\nu_{as}(SiO)$, respectively [86]. The spectra of the encapsulated $V^{IV}O(pic)_2-Y$ complexes as well as of this sample treated with an acetonitrile solution of urea hydroperoxide (UHP) were recorded. The most prominent peak characteristic of zeolite-Y was shifted to 496 cm^{-1} , and this small shift was explained by replacement of a part of the Na^+ cations by encapsulated $V^{IV}O(pic)_2$. The stretching vibrations of V–N bonds is obscured by the bending vibration of Si–O–Si and appears as a shoulder at about 450–470 cm^{-1} . New quite intense bands were observed in the Raman spectrum of $V^{IV}O(pic)_2-Y$ at 971, 1001, 1012, and 1028 cm^{-1} . The band at 971 cm^{-1} was assigned to $\nu(V=O)$ and there is significant difference from that observed in the zeolite-Y precursor (at 998 cm^{-1}). The other three bands were ascribed to vibrations associated to the picolinate ligands [86]. The Raman spectrum of the $V^{IV}O(pic)_2-Y$

treated with the acetonitrile solution of UHP showed new bands in the V–O_{peroxo} region at 549, 597, and 643 cm^{−1}, were assigned as due to encapsulated V^V-peroxo complexes, Raman spectroscopy being considered an adequate technique to characterize encapsulated vanadium peroxo complexes [86].

While the FTIR bands due to V^{IV}O(saloph) in V^{IV}O(saloph)-NaY were weak and masked by framework bands, in Al-MCM-41-V^{IV}O(saloph) the ligand bands were significantly more intense. The marginal shifts found in the bands due to C=N, C–O or C=C of the Schiff base ligand were assigned to changes in the geometry of V^{IV}O(saloph) due to encapsulation [65].

To establish the immobilization of vanadium complexes inside the pores of organically modified mesoporous silicas may not be an easy task. However, monitoring step by step the assembly of the complex inside the mesoporous silica may be helpful and V^{IV}O(L) complexes (L = H₂salten and derivatives with substituents in the ring) grafted on MCM-41 (see Scheme 19) were characterized in this way [65,66], namely with C=N bands at ca. 1640 cm^{−1}, and ν(V=O) at ca. 970 cm^{−1}.

The FTIR spectra of the V^{IV}O(salten) complex inside the channels of MCM-41 [65] and of Si-SBA-15 materials also confirmed the formation and integrity of the covalently anchored V^{IV}O(salten). The marginal shifts in the positions of the bands corresponding to C=N, C=C and C=O were also considered to be due to the immobilization of the complex.

3.3. Thermogravimetric analysis

Thermogravimetric analysis (TG or TGA) of polystyrene-anchored complexes under oxygen atmosphere may be useful to understand the nature of the ligands bound to the metal centre and through the weight of the final residue at ca. 800 °C, in the form of V₂O₅, estimate the amount of metal ion coordinated to the polystyrene-anchored ligand. In favorable cases the pattern of the thermogram may confirm the presence of a particular coordinated ligand.

With zeolites or MCM materials the clear observation of weight loss depends on the loading of the organic ligand of the catalysts, information that is also obtained from elemental analysis data. If the loading is too low, the loss of mass may be practically imperceptible. The temperatures where decomposition/combustion of the ligands occur and the weight losses observed also give indication if the complex is encapsulated or grafted inside the cavities, and of its loading [11].

Globally TG may show three stages of weight loss: (1) due to loss of condensed and physically adsorbed water (below ca. 400 K), (2) due to loss of chemisorbed water in the form of OH groups (below ca. 670 K) (3) the third stage corresponds to combustion of encapsulated/grafted organic molecules. Depending on the ligand and on the type of binding to the support, the weight loss stages may be separated or superimposed. For example the thermal decomposition of the Si-MCM-41-V^{IV}O-(salten) complex was observed in two steps [65]. The former (<100 °C) is due to desorption of water while the latter, at 350–600 °C, was due to decomposition/combustion of salten complex.

3.4. Adsorption studies

Most heterogeneous catalysts, including metal oxides, supported metal catalysts and zeolites are porous materials with specific surface areas ranging from 1 to 1300 m²/g. The surface area, pore volume and average pore size of such porous catalysts are normally correlated to the number of active sites available for catalysis, the diffusion rates of reactants and products in and out of these pores, and the deposition of coke and other contaminants. The most common method used to characterize the

structural parameters associated with pores in solids is via the measurement of adsorption–desorption isotherms, which involves the measurement of adsorption of a gas, typically N₂, as a function of its partial pressure. The most widely used technique for estimating surface area is the BET method [87], and the values obtained by sample weight may be designated by S_{BET}. Pore volume and pore radius may also be obtained from the adsorption measurements.

Four types of adsorption isotherms are usually found for catalysts, as defined by IUPAC [88]: type I, characteristic of microporous solids (pores < 2 nm), where pore filling takes place without capillary condensation, and is indistinguishable from the monolayer formation process. Type II, typical of macroporous solids (pores > 50 nm), where the prevailing adsorption processes are the formation of a monolayer at low relative pressures, followed by gradual and overlapping multilayer adsorption as the pressure is increased. Type IV, often seen in mesoporous solids (pores: 2–50 nm), where condensation occurs sharply at a pressure determined by Kelvin-type rules. Type VI, corresponding to uniform ultramicroporous solids, where the pressure at which adsorption takes place depends on surface–adsorbate interactions, and shows isotherms with various steps, each corresponding to adsorption on one group of energetically uniform sites.

N₂ adsorption–desorption isotherms of MCM-41, CP-MCM-41 and V-MCM-41 normally exhibit a typical type-IV isotherm with small hysteresis for neat MCM-41, CP-MCM-41 and V-MCM-41, characteristic of a mesoporous structure. The relative pressure at which pores are filled is shifted to a lower value for the modified samples in comparison to the parent materials, resulting in decrease in S_{BET}, pore volume and pore diameter. From a N₂ sorption study the S_{BET} of MCM-41 is 1280 m²/g, the mesopore volume is 1.19 mL/g and the average pore diameter was calculated as 3.0 nm using the Barrett–Joyner–Halenda (BJH) method [66].

Părvulescu et al. prepared several vanadium incorporated mesoporous silicate catalysts by either direct hydrothermal synthesis or impregnation, and measured the N₂ adsorption–desorption isotherms. These have the characteristic shape of MCM-41 materials and show an inflection in the P/P₀ range of 0.3–0.38, representative of the capillary condensation within uniform mesopores. All samples showed a high surface area (878–1245 m²/g), and the pore size distribution obtained by BJH method gave values in the range of 2.5–3.1 nm. The increase of the vanadium content due to the extra-framework V species and the use of NH₄OH, leading to less well organized structures, decreased the specific surface area of these materials [84].

The textural properties (surface area and pore size) of the complex [V^{IV}O(salten)] (see 45 and 46 in Scheme 19) grafted on MCM-41 [65] and SBA-15 [64] through an organic spacer were determined from the N₂-sorption studies at 77 K. On modifying MCM-41 with 3-CPTES [(3-glycidyloxypropyl)-triethoxysilane] the surface area of MCM-41 decreased from 1000 to 850 m²/g (980–820 m²/g from SBA-15 to Si-SBA-15 [64]) and the pore size was reduced from 3 to 2.4 nm (8.0–7.6 nm from SBA-15 to Si-SBA-15). Upon further immobilizing [V^{IV}O(salten)] to produce 46, a reduction in the surface area from 850 to 700 m²/g and pore size from 2.4 to 1.6 nm was observed. The reduction in the surface areas and pore sizes was considered to be due to the lining of the walls of Si-MCM-41 (and Si-SBA-15) with the organic moieties [64,65]. In a recent study it was reported that the surface area of MCM-41 decreased from 1280 to 983 m²/g in CP-MCM-41, and upon grafting [V^{IV}O(salten)] the surface area decreased to 584 m²/g. The corresponding pore volumes were: 1.19, 1.03 and 0.68 mL/g and the pore diameters: 3.1, 2.6 and 2.0 nm [66]. These inorganic–organic hybrid materials proved to be efficient catalysts, better than their neat counterparts as the active species are covalently bound to the support and place no restrictions on the pore size.

The oxovanadium complexes bearing the ligand Ph-DAB-(CH₂)₃R [R=Si(OEt)₃] (L), were grafted in ordered MCM-41 (**52** in Scheme 23(A)). The MCM-41 starting material showed type IV N₂ adsorption isotherm, and the specific surface area (*S*_{BET}) and total pore volume are 1046 m²/g and 0.87 mL/g, respectively, while the solid **52**, with the grafted V complex showed a lower N₂ uptake corresponding to a decrease in *S*_{BET} of 22%. This and other data indicate that the complex was successfully supported on the internal surfaces of the mesoporous MCM-41 [63].

For zeolite-Y, zeolite-V^{IV}O-Y and four zeolite V^{IV}O(L)-Y (L=tetradentate Schiff base) encapsulated complexes, the surface area and pore volume were determined by N₂ adsorption isotherms, and the values reported were: 545 m²/g and 0.31 mL/g (zeolite-Y), 516 m²/g and 0.29 mL/g (zeolite-V^{IV}O-Y) and in the range 441–464 m²/g and 0.17–0.20 mL/g, respectively, for the V^{IV}O(L)-Y encapsulated complexes. Therefore, there is a drastic reduction of surface area and pore volume of zeolites on encapsulating the V^{IV}O-complexes. Since as shown by the XRD pattern, the zeolite framework structure is not affected by encapsulation, the reduction of surface area and pore volume provided direct evidence for the presence of complexes in the zeolite cavities [48]. The same was found for the set of four complexes **34–37** (Scheme 17) with [14]aneN₄ ligands [61]. The *S*_{BET} and micropore volume were also determined for zeolite-NaY, 735 m²/g and 0.32 mL/g being reported. Upon the encapsulation of [V^{IV}O(salen)] these values became 358 m²/g and 0.18 mL/g [85].

Metal phthalocyanine (Pc) complexes encapsulated in zeolite-Y by the “template synthesis method” gave also a decrease of *S*_{BET} upon encapsulation, 388 m²/g for a support with 3.0 Pc molecules/unit cell, and 448 m²/g with 1.0 Pc molecules/unit cell, consistent with the expectation that the higher the amount of complex encapsulated, the lower the *S*_{BET} [60]. Similar conclusions were obtained encapsulating V^{IV}O(L) complexes with 12-membered macrocyclic ligands [45]: the inclusion of V^{IV}O(12-membered macrocyclic) complexes dramatically reduced the adsorption capacity and the surface area of the zeolite, the lowering of the nanopore volume and surface area indicating the encapsulation of the complexes and not their binding on the external surface of the zeolite.

3.5. Powder X-ray diffraction

X-ray diffraction (XRD) is commonly used to determine the structure and composition of the catalyst. Powder X-ray diffraction patterns of crystalline samples show diffraction peaks and it is typically limited to the identification of specific lattice planes that produce peaks at their corresponding angular positions 2θ determined by Bragg's law. With zeolite-Y these are normally measured in the range 10–70°, and with MCMs in the range ca. 1–10°.

What is mainly checked with supported catalysts after the procedures used for the production of the heterogenized complexes, or after the catalytic reactions, is if there is any loss in crystallinity and/or variations in relative peak intensities and/or morphology of the solid material [45,49–52,61,66]. Due to the low loading of the complexes, no new peaks are expected to show up.

Upon functionalization and metal complex loading a decrease in intensity with broadening of peaks may occur indicating the introduction of slight disorder in the zeolite or the mesoporous materials. The introduction of complexes and procedures used to do it may distort the regular crystalline arrays of the material or the long-range order of the MCM-41 mesostructure. This may also become more significant when larger or more abundant organic species are added.

In the XRD pattern of faujasite zeolite-NaY typically the relative intensities of the (3 3 1), (3 1 1), (2 2 0) peaks are observed,

namely to check if there is significant cation redistribution due to the encapsulation of the catalyst [45,50–52,61]. In almost all reported cases no significant variation was observed in the diffraction pattern due to the encapsulation procedures. For example in zeolite-Y and zeolite-V^{IV}O-Y, the relative intensities of the peaks varied in the order (3 3 1) > (2 2 0) > (3 1 1), indicating a random distribution of the exchangeable cations within the zeolite lattice. Upon introduction of ligand H₂saloph, producing zeolite-[V^{IV}O(saloph)] (**24** in Scheme 15) the peak intensities varied in the order: (3 3 1) > (3 1 1) > (2 2 0), suggesting displacement of cations in the supercages by the complexes. The XRD patterns of Al-MCM-41 revealed that the mesoporous structure was retained even after encapsulation of [V^{IV}O(saloph)] [51].

The XRD pattern of MCM-41 shows typically three to five reflections between $2\theta=2^\circ$ and 5° , although samples with more reflections have also been reported [89,90]. The reflections are due to the ordered hexagonal array of parallel silica tubes and can be indexed assuming a hexagonal unit cell as (1 0 0), (1 1 0), (2 0 0), (2 1 0) and (3 0 0). Since the materials are not crystalline at the atomic level, no reflections at higher angles are observed.

For example, the XRD patterns of Si-MCM-41, C1-Si-MCM-41 and Si-MCM-41-[V^{IV}O(salten)] **45** have been measured [65]. The XRD pattern of Si-MCM-41 shows a very intense peak assigned to reflections at (1 0 0) and two additional peaks with low intensities at (1 1 0) and (2 0 0) reflections. Some loss in the intensity of the peaks was observed upon modification with 3-CPTES, showing that though there is some reduction in the crystallinity of Si-MCM-41, the mesoporosity of Si-MCM-41 is retained. No further loss in the intensity of the peak at (1 0 0) reflection was observed on immobilizing [V^{IV}O(salten)] producing **45** (Scheme 19), but the peaks at (1 1 0) and (2 0 0) reflections were not observed upon this modification. In contrast, after using a similar procedure for Si-SBA-15, no significant loss in the intensity was observed on immobilizing the [V^{IV}O(salten)] complex producing **46** [64].

The attenuation of peak intensities upon binding of a metal complex to MCM materials does not necessarily correspond to a loss of order, but to a likely reduction in the X-ray scattering contrast between the silica walls and pore-filling material. The peak intensity reduction also depends on the amount of ligand and metal content [63].

The X-ray diffraction patterns of high quality were recorded to study zeolite-Y, zeolite-V^{IV}O-Y obtained by the ion exchange method and two V^{IV}O(salen)-Y solids, one obtained by the impregnation method (IM), the other by encapsulation [85]. The diffraction patterns were indexed by suitable programs. The (2 1 0) reflection represents the exchanged zeolite phase (lower cavity volume), and considering its low intensity and the presence of high intensity (1 1 1) reflection (which corresponds to non-exchanged zeolite, with higher cavity volume), it was concluded that only partial exchange occurred in the zeolite cavities, its extent depending on the reaction time. Based on (1 1 1) or (2 1 0) reflections a non-linear least squares program was used to obtain refined lattice volumes. An increase in reaction time resulted in a decreased lattice volume, confirming these conclusions [85]. The cell volume for the [V^{IV}O(salen)]-Y samples produced by encapsulation is larger than that for V^{IV}O-Y, confirming the effective encapsulation of the ligand. However, it could not be concluded that [V^{IV}O(salen)] was encapsulated by the impregnation method since no (2 1 0) reflection was observed. Its cell volume did not differ significantly from that of zeolite-NaY [85].

3.6. Field emission-scanning electron microscope (FE-SEM) and X-ray fluorescence (XRF) studies

Field emission-scanning electron microscope (FE-SEM) in combination with X-ray fluorescence (XRF) may provide useful

information on the anchoring of ligands and complexes and have been extensively used [33–35,39–44] namely to examine polystyrene bound vanadium catalysts to observe the morphological changes that might have occurred upon the anchoring processes.

Normally, due to poor loading of the metal complexes, by FE-SEM it is not possible to obtain accurate information on the morphological changes in terms of exact orientation of ligands coordinated to the metal ion. Typically, it is observed that e.g. pure polystyrene beads have a smooth and flat surface and upon anchoring the ligands and complexes slight roughening of the top layers may be noticed. Higher roughening is observed in the particles with anchored complexes probably due to the fact that interaction of metal ion with the anchored ligand results in the formation of a more rigid geometry. After swelling in solvents e.g. acetonitrile, often opening of the pores can be visualized due to swelling of the beads. Through the pores the substrates may enter and reach the active catalyst sites [29].

Additionally FE-SEM may be observed along with X-ray fluorescence profiles, namely by dispersive X-ray analysis (EDX), which is an excellent analytical technique to obtain the elemental analysis choosing a particular region of the surface of the solid particles. The detection of a significant metal content along with nitrogen gives indication of the effective anchoring of the complex to the PS-matrix [29,32,41].

SEM has also been applied to $[\text{V}^{\text{IV}}\text{O}(\text{L})]$ -alumina and $[\text{V}^{\text{IV}}\text{O}(\text{L})]$ -Y **26** of Scheme 15 [52]. The vanadium loading in alumina- $[\text{V}^{\text{IV}}\text{O}(\text{L})]$ is ca. 20 times higher than in $[\text{V}^{\text{IV}}\text{O}(\text{L})]$ -Y, and while the former showed variation in the surface of the alumina after the adsorption of the $[\text{V}^{\text{IV}}\text{O}(\text{L})]$, due to the low loading of $[\text{V}^{\text{IV}}\text{O}(\text{L})]$ in $[\text{V}^{\text{IV}}\text{O}(\text{L})]$ -Y (**26**), confirmed by FAAS, no changes could be detected by SEM observations.

Auger electron spectroscopy (AES) and X-ray photoelectron spectroscopy (XPS) are close relatives of EDS, utilizing ejected electrons. Information on the quantity and kinetic energy of ejected electrons is used to determine the binding energy of these liberated electrons, which is element-specific and allows chemical characterization of a sample. XPS may provide information about relative concentrations of elements in the upper ~ 40 – 50 \AA – thick layer of the sample ($\sim 1\%$ of the crystal), while XRF analysis allows to estimate bulk amounts of elements.

A comparison of the Si/V surface concentration ratios was made by XPS and XRF among zeolite-Y supported $\text{V}^{\text{IV}}\text{O}$ -picolinate and $\text{V}^{\text{IV}}\text{O}$ -salen complexes obtained either by encapsulation using the flexible ligand (FL) method, or grafted by the template synthesis method (TS). The anchored materials possessed higher external surface content of vanadium in comparison with the encapsulated samples, despite lower vanadium loading of the grafted samples [50]. Thus, the comparative XPS/XRF study indicates a more reliable confirmation of intrazeolitic complex location.

XPS studies also helped establishing that the $[\text{V}^{\text{IV}}\text{O}(\text{bipyridine})_2]^{2+}$ -Y complexes are intrazeolitic and homogeneously distributed across the zeolite crystals [62]. XPS of encapsulated $[\text{V}^{\text{IV}}\text{O}(\text{saloph})]$ -Y (**24**) and Al-MCM-41- $[\text{V}^{\text{IV}}\text{O}(\text{saloph})]$ indicated that in encapsulated complexes the spectra are weak and that the complexes are inside the cages [51].

To elucidate the pore structure of MCM-41 transmission electron microscopy has also been used [83,90,91]. Most MCM-41 samples not only showed ordered regions but also disordered regions, lamellar and fingerprint-like structures [92]. TEM images of V-MCM-41 materials, obtained both from tetraethylorthosilicate (TEOS) and sodium silicate, showed a very regular array of mesoporous channels in a hexagonal organization. Comparing the XRD patterns and TEM images of V-MCM-41 samples obtained by direct synthesis and impregnation, the pore structure is more disordered in the latter case [84].

3.7. X-ray absorption spectroscopy

X-ray absorption spectroscopy (XAS) normally involves the measurement of the x-ray absorption coefficient and includes both extended X-ray absorption fine structure (EXAFS) and X-ray absorption near edge structure (XANES). EXAFS spectra are displayed as graphs of the absorption coefficient of a given material versus energy, typically in the 500–1000 eV range, beginning before an absorption edge of an element in the sample. The normalized absorption spectra are often called XANES spectra. These spectra can be used to determine the average oxidation state of the element in the sample, and the XANES spectra are also sensitive to the coordination environment of the absorbing atom in the sample. The most notable feature in the V K-edge XANES spectrum is electronic transitions from 1s to d orbital, s (non-dipole), and p-like (dipole-allowed) empty states. The valence and the local coordination environment are correlated with the nature of the pre-edge peak in the V K-edge XANES spectra, and the intensity of the pre-edge peak is greatly affected by the coordination number and symmetry of the vanadium species. Usually, a higher intensity of the pre-edge peak implies higher dispersion and lower coordination [93].

The vanadium K-edge XAFS data were measured for impregnated (IM) $\text{V}^{\text{IV}}\text{O}(\text{pic})_2$ -IM-Y, $\text{V}^{\text{IV}}\text{O}(\text{pic})_2$ -FL-Y obtained by the flexible ligand method, and neat compounds $\text{V}^{\text{IV}}\text{O}(\text{pic})_2 \cdot \text{H}_2\text{O}$ and $\text{V}^{\text{IV}}\text{O}(\text{pic})_2(\text{py})$. The pre-edge and near-edge features in XANES spectra were almost the same for the impregnated and encapsulated samples, and similar to those of $\text{V}^{\text{IV}}\text{O}(\text{pic})_2 \cdot \text{H}_2\text{O}$. The pre-edge peak position at 5447.9 eV is consistent with an oxidation state of IV. Upon comparison of the XANES of the $\text{V}^{\text{IV}}\text{O}(\text{pic})_2$ -FL-Y sample with those of the two reference compounds it was concluded that in the encapsulated sample the structures around the vanadium atom are square pyramidal or distorted octahedral coordination [50]. Difference in the Fourier transforms between the reference compound $\text{V}^{\text{IV}}\text{O}(\text{pic})_2 \cdot \text{H}_2\text{O}$ and the $\text{V}^{\text{IV}}\text{O}(\text{pic})_2$ -FL-Y sample is concerned with changes in the second shell, where the second peak developed more in the case of the reference complex $\text{V}^{\text{IV}}\text{O}(\text{pic})_2 \cdot \text{H}_2\text{O}$. Comparison of raw EXAFS oscillations for the two reference complexes and the encapsulated one was explained in terms of coordination of zeolite-OH groups to the vanadium complexes forming a six-coordinated bis-picolinate structure [50].

Treatment of the $\text{V}^{\text{IV}}\text{O}(\text{pic})_2$ -FL-Y complex with an UHP solution in acetonitrile generated peroxovanadium species. The structure of this species was studied by UV-vis, Raman and XAFS spectroscopy, which suggested the formation of a $\text{V}^{\text{V}}\text{O}(\text{O}_2)(\text{pic})$ complex, which may be the active intermediate for various oxidations promoted by the catalysts [86]. XANES spectra $\text{V}^{\text{IV}}\text{O}(\text{pic})_2$ -FL-Y before and after treatment with the UHP solution were measured. The pre-edge peak for $\text{V}^{\text{IV}}\text{O}(\text{pic})_2$ -FL-Y treated with UHP was at 5468.4 eV, which was higher by $\sim 0.5 \text{ eV}$ than that for the untreated sample. Shift of the pre-edge peak (the value is higher by $\sim 4.5 \text{ eV}$ than that for vanadium foil) reflects the oxidation of V(IV) to V(V) by the treatment of the sample with UHP. The reference compounds showed the $1s \rightarrow 4p$ transition peak at 5485.0 eV for $\text{H}[\text{V}^{\text{V}}\text{O}(\text{O}_2)(\text{pic})_2] \cdot \text{H}_2\text{O}$ and 5485.7 eV for $\text{V}^{\text{V}}\text{O}(\text{O}_2)(\text{pic})_2 \cdot 2\text{H}_2\text{O}$ [86].

3.8. Electronic spectroscopy

Electronic spectra of the heterogenized complexes have been recorded either (i) by dispersing the sample as Nujol[®] mulls layered on quartz plates, or on the inside of cuvettes and using a double-beam spectrophotometer, or (ii) using reflectance methods. Diffuse reflectance spectra (DRS) are normally more sensitive than the use of Nujol[®] mulls, and the weak d–d transitions ($\epsilon < 100$) of $\text{V}^{\text{IV}}\text{O}$ -catalysts are normally not observed by this procedure. Additionally, due to their poor loading in the solid supports, even ligand to metal

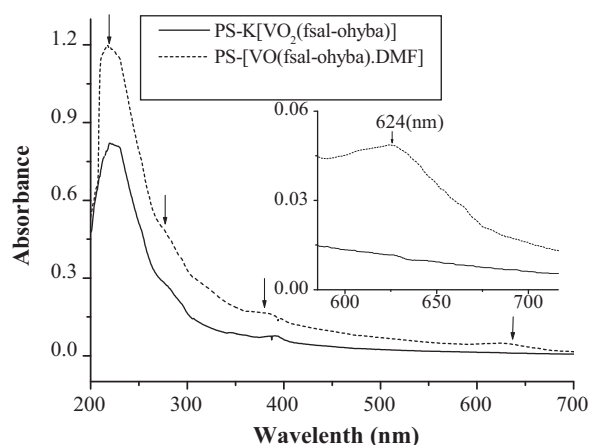


Fig. 1. Electronic spectra of the polymer-anchored complexes: PS-K[VVO₂(fsal-ohyba)] (**2**) (solid line) and PS-[VO(fsal-ohyba).DMF] (**1**) (dashed line) [30].

charge transfer (lmct) bands sometimes are not detected. Nevertheless, Nujol® is a good dispersion medium, it is simple to apply and does not require a reflectance spectrophotometer, therefore it was extensively used to characterize heterogenized complexes dispersed in Nujol® [37–42,49,53–59].

Most polystyrene-bound complexes show ligand bands similar to those observed in neat as well as polymer-bound ligands. As lmct imine bands and particularly d–d transitions are not intense, they require relatively high concentrations of metal complexes and such transitions either are observed as weak bands or not observed at all in polymer-anchored complexes. However, there are favorable cases where they have been recorded. The electronic spectrum of PS-[V^{IV}O(fsal-ohyba).DMF] (**1**) [30] showed the d–d band as a weak shoulder at 517–630 nm, and the lmct band at ca. 395 nm. The dioxo complex, PS-K[VVO₂(fsal-ohyba)] (**2**) [30] also displayed weak lmct bands in the same region (Fig. 1).

The electronic spectra of the [V^{IV}O(Salen)]-Y (**20**) were recorded as Nujol mulls between quartz plates and the bands observed at 276 and 360 nm were quite similar to the reported values at 285 and 365 nm for V^{IV}O(Salen) in CH₂Cl₂ [49]. UV–vis spectra of the neat V^{IV}O(Pc) (Pc = phthalocyanine) complexes showed two resolved Q-bands at 618 and 678 nm, while the encapsulated V^{IV}O(Pc)-Y complexes showed bands at 650, 712 and 810 nm. The Q-bands red-shift in the order: V > Cu > Co. The resolution and shift in Q-bands in the encapsulated complexes were attributed to molecular isolation and distortion of Pc from planarity to a puckered geometry [60].

The presence of vanadium Schiff base complexes anchored on solids can be assessed by UV–vis. For example in the DRS of several samples, namely MCM-41, grafted with [V^{IV}O(salen)] complexes, the characteristic band appearing at ~360 nm is observed, confirming the presence of the anchored salen-complexes [69].

Four V^{IV} and V^V complexes with the tetradentate Schiff-base ligand (X₂-haacac – Scheme 15) were encapsulated in the nanopores of zeolite-Y. The DRS of these catalysts exhibit one broad band between 355 and 394 nm, assigned to an lmct transition. A weak band appeared at ca. 560 nm for the [V^{IV}O(X₂-haacac)]-Y complexes **27** [48]. Similar results were obtained for the set of four V^{IV}O-complexes **34–37** with [14]aneN₄ ligands encapsulated in zeolite-Y (Scheme 17). The DRS of all complexes exhibited one broad band at 355–394 nm, assigned to lmct transitions, and a weak band also appeared at ~580 nm [61]. A set of V^{IV}O-complexes with of 12-membered macrocyclic ligands having N₂O₂, N₂S₂ and N₄ donor atoms in the nanocavity of zeolite-Y were prepared by the FL method and their DRS spectra measured. The electronic spectra of all complexes exhibit one broad band at 360–390 nm, which was assigned to a lmct transition, and a weak band at 551–575 nm,

assigned to a d–d transition [45]. The DRS of these V^{IV}O-complexes before and after the heterogenization process are very similar, indicating that the complexes even after heterogenization maintain their geometry without significant distortion and their electronic surrounding [45,48,61].

The DRS of the [V^{IV}O(pic)₂]-Y (FL) sample exhibit bands at 740, 560 and 370 nm, which were assigned to the d–d bands I, II and III, respectively [94]. The bands resembled those of solutions of neat V^{IV}O(pic)₂. A band at ~270 nm was assigned to the ligand $\pi \rightarrow \pi^*$ transition, overlapping with the lmct of O to V^{IV}. This and the EPR data (see below) suggests only a small distortion of the VO(pic)₂ structure upon encapsulation [50]. It is known that vanadium can form monoperoxo and diperoxo complexes, which show absorption bands at 450–480 nm and 320–340 nm [95]. DRS in UV–vis region for the [V^{IV}O(pic)₂]-HL-Y treated (and non-treated) with UHP were measured. The increased intensity of the band centered at 475 nm was assigned as due to the oxidation of the encapsulated [V^{IV}O(pic)₂] complex to form monoperoxo species upon treatment with UHP [86].

3.9. EPR spectroscopy

Electron paramagnetic resonance (EPR) has been used to characterize V^{IV}O-species in several types of solid supports e.g. Al-substituted mesoporous silicas [96], encapsulated in zeolites [50,60,62,86,93,96] and covalently bound to a polystyrene matrix [e.g. 29,32,35,41,43] and mesoporous materials [e.g. 51,63,96].

One immediate advantage of V^{IV}O-heterogenized complexes as catalysts is that the metal coordination sites can be probed by means of EPR spectroscopy. In many cases satisfactory spectra can be obtained for powdered samples at room temperature without the use of solvent. The information provided by this technique can confirm if the synthesis of the catalyst was successful, namely if the metal ion is indeed encapsulated or anchored to the support.

It may also be probed if there is more than one type of environment around the V^{IV}-centre. In fact, from each experimental EPR spectrum of V^{IV}O-complexes the spin Hamiltonian parameters g_{\perp} , g_{\parallel} , A_{\perp} and A_{\parallel} (or g_x , g_y , g_z , and A_x , A_y and A_z) may be obtained by simulation using appropriate computer programs. The value of A_{\parallel} can be estimated ($A_{\parallel}^{\text{est}}$) using an additivity relationship proposed by Wüthrich [97] and Chasteen [98] with estimated accuracy of $\pm 1.5 \times 10^{-4} \text{ cm}^{-1}$. This value can be correlated to the number and type of binding groups in the equatorial position, since each donor-group has a specific contribution to the A_{\parallel} , and the sum of contributions of the four equatorial groups gives the value of $A_{\parallel}^{\text{est}}$ which may then be compared with the A_{\parallel} observed.

By comparison of shape/pattern of the spectra, and of the spin Hamiltonian parameters of the neat complexes in solution and encapsulated in zeolites [e.g. 50,51,60,62,99], relevant information may be obtained concerning the preparation of the immobilized complex, if it is in an oligomerized form or not, establish the binding mode or obtain indication on any confinement effects operating. For example, hydrated V^{IV}O-zeolite-Y species were prepared and its EPR spectrum recorded. It was concluded that the V^{IV}O²⁺ ions are largely located on type III sites in the large cavities bound to hydroxyl or O atoms ($g_{\perp} = 1.986$, $g_{\parallel} = 1.938$, $A_{\perp} = 74 \times 10^{-4} \text{ cm}^{-1}$ and $A_{\parallel} = 178 \times 10^{-4} \text{ cm}^{-1}$). Upon dehydration the spin Hamiltonian parameters change (to $g_{\perp} = 1.989$, $g_{\parallel} = 1.917$, $A_{\perp} = 78 \times 10^{-4} \text{ cm}^{-1}$ and $A_{\parallel} = 190 \times 10^{-4} \text{ cm}^{-1}$), but upon re-hydration the original parameters are restored [99]. The change of the EPR spectrum after introduction of a ligand and its similarity with the corresponding neat complex is a good proof of the encapsulation of the [V^{IV}O(ligand)] species inside the pores of zeolite-Y.

[V^{IV}O(saloph)] complexes were encapsulated in microporous zeolites-Y (forming **24**) and mesoporous Al-MCM-41 by the flexible

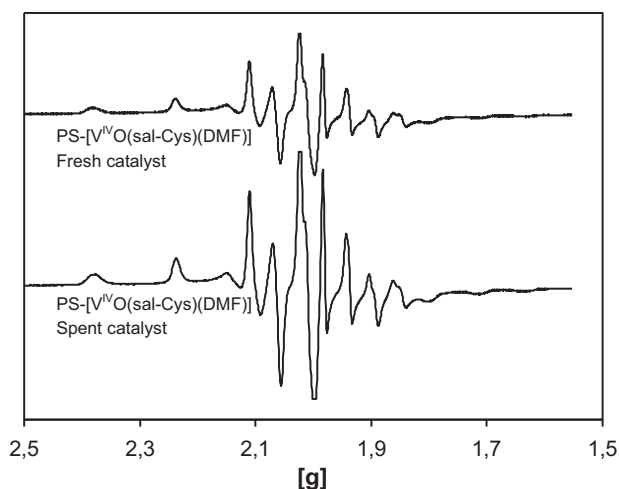


Fig. 2. EPR spectra of powdered samples of the fresh and spent catalysts PS-[V^{IV}O(sal-L-Cys)(DMF)] [29].

ligand method. The V content is ca. 40% higher in the MCM-41 and while the complexes are isolated and confined in the supercages of zeolite-Y, in MCM-41 the EPR signal is rather broad, indicating the existence of weak intermolecular interactions [51]. Interestingly the V-saloph species encapsulated in MCM-41 was more active than in zeolite-Y.

EPR was particularly useful to characterize the binding modes in powdered samples of many solid supports, particularly of polystyrene-anchored complexes [e.g. 29,32,35,41,43], namely to confirm that the vanadium centres are well dispersed in the polymer matrix, support (or not) the binding mode expected, and to check if the binding mode is preserved or not at the end of the catalytic reactions carried out. Clues on the formation of possible intermediates by addition of reagents may also be obtained. The relative intensities of the EPR spectra of the sample before and after the use of the catalyst may also give indication on the loss of metal during the reaction and recovery process, or if the V^{IV}O-centre was oxidized to V^V-species.

To elucidate the use of EPR for the characterization of PS-V^{IV}O complexes, Fig. 2 depicts EPR spectra of powdered samples of a fresh and spent catalyst. It may be seen that the two spectra are very similar, thus indicating that the catalyst recovered after use in a catalytic reaction has not suffered much change, at least as far as the amount of V^{IV}O-anchored and the binding mode are concerned.

3.10. Magnetic properties

Magnetic property measurements for V^{IV}O-compounds may be applied to sort out if there are significant interactions between neighboring V^{IV}O-centres. Additionally, in encapsulated or grafted matrices magnetization measurements may yield information on the loading of paramagnetic centres to the solid material. These techniques were not much applied to characterize heterogenized vanadium catalysts, but two representative examples will be mentioned.

Magnetic susceptibility measurements (from the EPR integrated signal intensities) were obtained for the [V^{IV}O(bipy)₂]-Y in the range ca. 4–300 K. According to Curie's law the reciprocal molar susceptibility of diamagnetic materials is proportional to the absolute temperature. For [V^{IV}O(bipy)₂]-Y the plot of the EPR integrated signal intensity was linearly related to the temperature, the straight line intersecting the abscissa at a Curie–Weiss temperature close to 0 K (at –3.96 K). This indicates a distribution of isolated V^{IV}-centres in [V^{IV}O(bipy)₂]-Y [62].

Magnetization data were collected using a SQUID (superconducting quantum interference device) magnetometer with powdered samples of non-supported complexes [V^{IV}O(acac)(L)]Cl {L = Ph-DAB-(CH₂)₃Si(OEt)₃}, as well as in the materials VO(acac)(L)-MCM-41 (**52** in Scheme 23(A)) and V^{IV}O(acac)-MCM-41. The analysis of the data using the spin-Hamiltonian model yielded vanadium concentrations of 0.93% and 2.06%, for **52** and V^{IV}O(acac)-MCM-41, respectively, in reasonable agreement with the analytical results (0.8 and 2.4 wt%, respectively). The discrepancies observed for the concentration values may be related to the presence of adsorbed molecular oxygen, whose influence is significant for samples with small total magnetic moment [63].

3.11. Solid state NMR spectroscopy

Under anisotropic conditions, NMR lineshapes for a quadrupolar nucleus are dominated by chemical shielding and 1st and 2nd order quadrupolar interactions [4]. First order quadrupole interaction lifts the degeneracy of the allowed 2I (seven in the case of ⁵¹V, I = 7/2) Zeeman transitions, giving rise to 7 equidistant lines, with the central line not affected by quadrupole interaction. The overall span of the spectrum is determined by the size of the nuclear quadrupole coupling constant C_Q, the deviations from axial symmetry and thus the shape of the spectrum being governed by the asymmetry parameter [4]. Static solid state NMR thus may provide the quadrupole coupling constant, which is related to the particular electronic environment of the V centre. The central component reflects the anisotropy of the chemical shift [4]. Magic angle spinning (MAS) of samples removes 1st order quadrupole interactions, a spinning side band manifold may be obtained from which the central transition δ_σ can be sorted out as the band the position of which remains unchanged when changing the spinning frequency.

NMR has not been much used to characterize vanadium heterogenized complexes and only a few representative examples will be mentioned.

The presence of distorted tetrahedral V species in VSiβ zeolites was confirmed by ⁵¹V NMR signals {δ_{iso}(MAS) = –633 ppm and δ_{iso}(static) = –580 ppm} characteristic of isolated vanadium ions with tetrahedral oxygen coordination [19], the distorted tetrahedral V species incorporated in microporous VSiβ zeolite being comparable to V species grafted on the surface of silica or incorporated in mesoporous matrices. Modifications in the distortion of tetrahedral V species after calcination and rehydration were confirmed by shifts of the ⁵¹V NMR signals from –633 to –698 ppm (MAS NMR) and from –580 to –605 ppm (wide-line NMR). In addition, the formation of octahedral V species was indicated by appearance of ⁵¹V NMR signals at –559 ppm (MAS NMR) and –350 ppm (wide-line NMR) [19].

The degree of functionalization i.e. the covalent linkage between the silanol groups and the organic moiety on the mesostructured materials can be monitored by means of ²⁹Si cross-polarization MAS NMR (CP-MAS NMR) spectroscopy. The spectrum of MCM-41 generally exhibits three resonance peaks at δ = –110, –101, and –92 ppm, corresponding to Q⁴ [siloxane, (SiO)₄Si], Q³ [single silanol, (SiO)₃Si(OH)] and Q² [geminal silanol, (SiO)₂Si(OH)₂] sites of the silica framework, respectively. Covalent binding makes the Q² signal disappear, decrease Q³ and concomitantly increase the Q⁴ intensity, which is due to consumption of isolated Si–OH and geminal silandiol during the condensation process [63,66]. Two resonance peaks due to the Si environments of Q⁴ (δ = –110 ppm) and Q³ (δ = –102 ppm) can be seen in the chloropropyl modified silica (CP-MCM-41, **XXVI** in Scheme 19). In addition to these two peaks, the sample displays two more resonance peaks at δ = –68 ppm, assigned to T³ [C–Si(OSi)₃], and at –57 ppm, attributed to T² [C–Si(OSi)₂(OH)], respectively. The existence T³ confirms that MCM-41 was modified by the organic moieties, and the appearance

of the Q^3 signal indicates the presence of some residual non-condensed OH groups attached to the silicon atom. Therefore ^{29}Si CP-MAS NMR provides direct evidence that the hybrid CP-MCM-41 sample consists of a highly condensed siloxane network with the organic group covalently bonded to the mesoporous silica [66].

In the ^{13}C CP-MAS NMR spectrum of CP-MCM-41 a sharp peak at 10.4 ppm was ascribed to the C atom bonded to Si [66]. The signal at 22.4 ppm corresponds to $-\text{CH}_2-$ carbon and the peak around at 50 ppm was assigned to the C atom attached to the Cl atom. Similar peaks were also observed for V-MCM-41 {V complex = $[\text{V}^{\text{IV}}\text{O}(\text{salen})]$ and derivatives, see Scheme 19} in the range of 0–40 ppm, this being due to partial change in the environment after the replacement of Cl by nitrogen. Peaks corresponding to the aliphatic and aromatic carbons of the Schiff base were also observed.

$[\text{V}^{\text{IV}}\text{O}(\text{acac})(\text{L})\text{Cl}]$ {L = Ph-DAB- $(\text{CH}_2)_3\text{Si}(\text{OEt})_3$ }, as well as in the materials $\text{VO}(\text{acac})(\text{L})\text{-MCM-41}$ (**52**) and $\text{VO}(\text{acac})\text{-MCM-41}$ (see Scheme 23(A)), grafting of ligand Ph-DAB- $(\text{CH}_2)_3\text{Si}(\text{OEt})_3$ into MCM-41 (producing **XXIX**) reduces the Q^3 and Q^2 resonances owing to the silylation of the surface and, concomitantly, increases the Q^4 resonance. This is consistent with esterification of the isolated SiOH groups by nucleophilic substitution at the Si atom in the organic compounds. The ^{29}Si CP-MAS NMR spectrum of **XXIX** displays two signals at $\delta = -54.8$, -59.4 ppm and a weak, broad signal at $\delta = -69.0$ ppm, assigned to T^1 , T^2 and T^3 organosilica species [$T^m = \text{RSi}(\text{OSi})_m(\text{OH})_{3-m}$], respectively, whereas the Q species only presents a peak at -108.3 ppm [63].

The ^{13}C CP-MAS NMR of the functionalized material **XXI** is very similar to that of the free ligand. A decrease in the intensity of the resonances of the $\text{SiO}-\text{CH}_2\text{CH}_3$ group at 16.5 ppm (CH_3) and 58 ppm (CH_2) is observed since the binding of the ligand to the surface of the host material takes place by the hydrolysis of such groups. The quality of the spectra of **52** is poor due to the presence of the paramagnetic complex, but the position of the peaks could be determined. Thus, the peaks observed in the range 0–75 ppm could be assigned to the CH_2 and CH_3 carbons of the propyl chain of the ligand. In **52** it was also possible to assign peaks at 9.6 (SiCH_2), 127.9 (phenyl-C) and 192.3 ppm ($\text{C}=\text{O}$) [63].

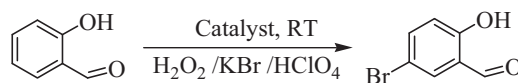
^{27}Al MAS NMR has also been measured for some Al-containing mesoporous silicas. Beside tetrahedral Al which dominates, small amounts of hexacoordinated Al are also present [96].

4. Catalytic activity studies

Vanadium(V) centres in complexes are usually strong Lewis acids due to their low radius/charge ratio [8] and act as catalysts in various organic transformations. Catalytic oxygen transfer reactions can be supported by a variety of oxygen donors, and the availability of active oxygen and nature of co-product(s) determine their practical utility, the most attractive oxidants, in terms of cost and environmental impact, being O_2 and H_2O_2 [100].

4.1. Oxidative halogenation

$\text{V}^{\text{VO}_2^+}$ species in acidic aqueous solution is a functional mimic of vanadium bromoperoxidases (VBrPO) [101], and e.g. oxidative bromination of 1,3,5-trimethoxybenzene (TMB) catalyzed by $[\text{V}^{\text{VO}}(\text{OMe})(\text{MeOH})(\text{sal-oap})]$ using H_2O_2 as oxidant was reported by Butler [6], the brominated product 2-bromo-1,3,5-trimethoxybenzene being obtained in good yield. Maurya et al. [53] reported the oxidative bromination of salicylaldehyde to 5-bromosalicylaldehyde (Scheme 24) catalyzed by $[\text{V}^{\text{VO}_2}(\text{sal-inh})]$ encapsulated in zeolite-Y, a process also mimicking vanadium bromoperoxidases (VBrPO) enzymes. By using H_2O_2 as an oxidant in the presence of KBr and HClO_4 the conversions were 27–34% with



Scheme 24. Oxidation product of salicylaldehyde.

ca. 87% selectivity after 4 h of reaction time for the major product formed, 5-bromosalicylaldehyde. The efficiency of the catalysts tested was $\text{NH}_4[\text{V}^{\text{VO}_2}(\text{sal-inh})]\text{-Y}$ (34%) > $\text{NH}_4[\text{V}^{\text{VO}_2}(\text{sal-oap})]\text{-Y}$ (26.8%) > $\text{Na}/\text{NH}_4\text{V}^{\text{VO}_3}\text{-Y}$ (22%). The presence of acid was essential for the catalytic oxidative bromination. $\text{NH}_4[\text{V}^{\text{VO}_2}(\text{sal-inh})]\text{H}_2\text{O}$ also catalyzed the oxidative bromination of salicylaldehyde with 45% yield of 5-bromosalicylaldehyde (with 90% selectivity) using $\text{H}_2\text{O}_2/\text{KBr}$ and HClO_4 in water or $\text{H}_2\text{O}_2/\text{KBr}$ in CH_3COOH , but fast decomposition of the complex occurred during reaction. As zeolite is not affected by small amount of acid used in catalytic experiment due to re-exchangable property of $\text{Na}^+/\text{NH}_4^+$ present in zeolite-Y with H^+ ion, it prevented decomposition of vanadium complexes present in the cavity of zeolite-Y.

Under the optimized reaction conditions, a maximum of 85% conversion of salicylaldehyde with the polymer supported complex $\text{PS-K}[\text{V}^{\text{VO}_2}(\text{sal-inh})(\text{im})]$ and ca. 82% with $\text{PS-K}[\text{V}^{\text{VO}_2}(\text{sal-bhz})(\text{im})]$ was achieved. Addition of more HClO_4 further improved the conversion of salicylaldehyde, but the selectivity for formation of 5-bromosalicylaldehyde decreased sharply and the supported complexes started to decompose. This decomposition could, however, be minimized when HClO_4 was added stepwise in about four equal portions. Other non-oxidizing acids such as H_2SO_4 were similarly tested successfully giving comparable results. Spent catalysts exhibited slightly lower conversions than fresh ones (Table 1). Noteworthy, these results with PS-anchored catalysts were better than those with the complexes encapsulated in zeolite-Y [44]. Successive addition of HClO_4 in four equal portions also helped in improving the stability of the catalyst when using $\text{PS-}[\text{VO}(\text{hmbmz})_2]$ and provided quantitative conversion of salicylaldehyde, being selective for the formation of 5-bromosalicylaldehyde. The polymer support acts as a kind of protein mantle and its inertness towards HClO_4 provides extra stability to the complex during the catalytic reactions [82].

4.2. Oxidation of organic sulfides

Many vanadium complexes catalyze the oxidation of organic sulfides to sulfoxides [9,10], a reaction also promoted by vanadium haloperoxidase enzymes. Organic sulfides have electron-rich sulfur atoms which undergo electrophilic oxidation giving sulfoxide; upon further oxidation sulfones are formed (Scheme 25).

Data on conversion and selectivity of products upon the oxidation of mps and dps by aqueous H_2O_2 using various supported vanadium complexes as catalysts are given in Table 2. Most vanadium catalysts are good/excellent for sulfide conversion with high

Table 1

Conversion of salicylaldehyde and selectivity data for 5-bromosalicylaldehyde [53].

Catalyst	% Conv.	TOF	% Selectivity	
			5-Brsal	Other
$\text{PS-K}[\text{V}^{\text{VO}_2}(\text{sal-inh})(\text{im})]$	85	775	90	10
$\text{PS-K}[\text{V}^{\text{VO}_2}(\text{sal-inh})(\text{im})]^a$	81	–	90	10
$\text{PS-K}[\text{V}^{\text{VO}_2}(\text{sal-inh})(\text{im})]^b$	79	–	87	13
$\text{PS-K}[\text{V}^{\text{VO}_2}(\text{sal-bhz})(\text{im})]$	82	800	90	10
$\text{PS-K}[\text{V}^{\text{VO}_2}(\text{sal-bhz})(\text{im})]^a$	79	–	88	12
$\text{PS-K}[\text{V}^{\text{VO}_2}(\text{sal-bhz})(\text{im})]^b$	76	–	86	14
$\text{K}[\text{V}^{\text{VO}_2}(\text{sal-inh})(\text{H}_2\text{O})]$	54	60	87	13
$\text{K}[\text{V}^{\text{VO}_2}(\text{sal-bhz})(\text{H}_2\text{O})]$	51	62	85	15

^a First cycle of used catalyst.

^b Second cycle of used catalyst.

Table 2Conversion of sulfides, TOF and product selectivity data^a.

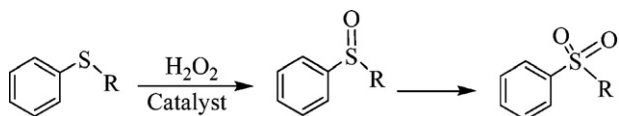
Complexes	Substrate	% Conv.	TOF (h ⁻¹)	% Selectivity	
				Sulfoxide	Sulfone
PS-K[V ^V O ₂ (sal-inh)(im)]	mps	98	589	97	3
PS-K[V ^V O ₂ (sal-inh)(im)] ^b	mps	93	–	97	3
PS-K[V ^V O ₂ (sal-inh)(im)] ^c	mps	90	–	99	1
PS-K[V ^V O ₂ (sal-bhz)(im)]	mps	98	638	98	2
PS-K[V ^V O ₂ (sal-inh)(im)] ^b	mps	95	–	98	2
PS-K[V ^V O ₂ (sal-inh)(im)] ^c	Mps	89	–	100	0
PS-[V ^{IV} O(sal-hist)(acac)]	mps	80	91	65	35
PS-[V ^V O ₂ (sal-hist)]	mps	94	114	64	36
PS-[V ^{IV} O(sal-hist)(acac)]	mps	67	29	73	27
PS-[V ^V O ₂ (sal-hist)]	mps	60	20	69	31
PS-[V ^{IV} O(hpbmz) ₂]	mps	77	72	77	23
[V ^V O ₂ (sal-ambmz)]-Y	mps	96	135	97	3
[V ^{IV} O(sal-oaba)(H ₂ O)]-Y	mps	93	598	97	3
[V ^{IV} O(tmbmz) ₂]-Y	mps	94	281	89	11
[V ^{IV} O(tmbmz) ₂]-Y	mps	92	117	73	27
[V ^{IV} O(MeOsal- <i>m</i> -xylenediam)]-Y	mps	92	–	78	14

^a Refer to text for references concerning catalysts.^b First cycle of used catalyst.^c Second cycle of used catalyst.

turn over frequency (TOF) along with good selectivity towards sulfoxide. Polymer-supported complexes PS-[*mer*-V^{IV}O(sal-ea)], PS-[*mer*-V^{IV}O(sal-pheol)], PS-[*mer*-V^{IV}O(sal-hisol)] and PS-[*mer*-V^{IV}O(sal-phe)] gave 81–91% conversion of methyl phenyl sulfide to sulfoxide upon oxidation with TBHP in 1.5 h where the enantiomeric excess of mps was as high as 40% with PS-[*mer*-VO(sal-hisol)] [28]. The enantioselectivity achieved with these PS-anchored catalysts was similar to that of the corresponding neat complexes, but rates of oxidation were slightly lower.

[V^{IV}O(MeOsal-*m*-xylenediam)]-Y exhibited only 34% conversion in one day but this increased to 92% after ca. four days [52]. Blank reactions using mps (1.24 g, 10 mmol), aqueous 30% H₂O₂ (2.27 g, 20 mmol) and acetonitrile (15 mL) may result in ca. 35% conversion with sulfoxide to sulfone selectivity of 68:32. Blank reactions for diphenyl sulfide under similar conditions gave only ca. 5% conversion with selectivity of 57:43. It must be emphasized that in these blank reactions the conversion of sulfide varies with the quality of acetonitrile and temperature, and for very pure solvent it may be negligible. However, the sulfoxide to sulfone ratios does not vary much. Thus, it may be stated that the supported catalysts not only enhance the conversion of organic sulfides but also enhance the selectivity towards the formation of sulfoxide.

MCM-41 supported complex **53** (with two different types of anchoring) and same complex supported on modified ultra stable zeolite-Y were used for the oxidation of mps and (2-ethylbutyl)phenyl sulfide by drop wise addition of either TBHP or 30% H₂O₂ at 273 K. All catalysts, homogeneous and heterogenized, were active and highly selective in conversion to sulfoxides, conversion of ca. 95–99% being obtained in 1 h for almost all reactions, but poor enantioselectivity was achieved (<10%) and the e.e.'s not changing during the reaction [70]. Globally the immobilized complexes were more active than the neat ones, and these could be reused in repeated cycles, although leaching was detected. For all these heterogenized catalysts, a high selectivity was observed for bulky substrates, this having been attributed to molecular sieving effects (reactants size and selectivity effects).

**Scheme 25.** Oxidation of organic sulfides. R = CH₃–: methyl phenyl sulfide = mps, R = C₆H₅–: diphenyl sulfide = dps.

The removal of sulfur compounds from petroleum products has attracted the attention of many researchers to fulfill the demand of environment friendly fuels. The oxidation of model organosulfur compounds (see Table 3) with sulfur concentrations of 500 ppm was tested in heptane and PS-[V^{IV}O(fsal-dmen)(acac)] and PS-[V^VO₂(fsal-dmen)] were used as catalysts in presence of 30% H₂O₂. The results are summarized in Table 3. It is clear from the table that polystyrene-supported catalysts are significantly more effective in oxidizing organic sulfur than their corresponding neat complexes, having the advantage of being more easily recovered from the reaction mixture [42].

4.3. Oxidation of phenol

As the hydroxyl group on phenol is *ortho* and *para* directing, the catalytic oxidation of phenol usually gives two products: catechol (cat) and hydroquinone (Hq). In some cases further oxidation also occurs to form *para*-benzoquinone (Pbq) (Scheme 26). Liquid phase hydroxylation of phenol by H₂O₂ to a mixture of catechol and hydroquinone in acetonitrile was reported using a wide range of vanadium complexes encapsulated in zeolite-NaY. Table 4 presents conversion of phenol and product selectivity for some of these.

Under “optimized reaction conditions for NH₄[V^VO₂(sal-inh)]-Y and NH₄[V^VO₂(sal-oap)]-Y ca. 26% conversion of phenol with catechol (85 and 77% selectivity, respectively) as major product was obtained after 6 h [59]. Under similar conditions, [V^{IV}O(sal-1,3-pn)]-Y showed the highest conversion after 6 h of 34%, [V^{IV}O(salen)]-Y and [V^{IV}O(saldien)]-Y had comparable catalytic activity, while [V^{IV}O(sal-1,2-pn)]-Y had the poorest performance

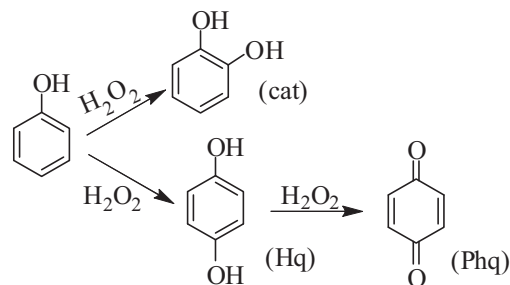
**Scheme 26.** Typical oxidation products of phenol: catechol (cat), hydroquinone (Hq) and *p*-benzoquinone (Phq).

Table 3
Desulfurization and reaction products using the anchored oxido- and dioxidovanadium catalysts: PS-[V^{IV}O(fsal-dmen)(acac)] and PS-[V^VO₂(fsal-dmen)] (0.050 g), 30% H₂O₂ (oxidant:substrate molar ratio of 3:1) at 60 °C [42].

Catalyst	Sulfur containing compound	Sulfur content (ppm)		Sulfur removal (%)
		Initial amount	After desulfurization	
PS-[V ^{IV} O(fsal-dmen)(acac)]	Thiophene	500	65.5	86.9
PS-[V ^{IV} O(fsal-dmen)(acac)]	Benzothiophene	500	63	87.4
PS-[V ^{IV} O(fsal-dmen)(acac)]	Dibenzothiophene	500	60.5	87.9
PS-[V ^{IV} O(fsal-dmen)(acac)]	2-Methylthiophene	500	57.5	88.5
PS-[V ^V O ₂ (fsal-dmen)]	Thiophene	500	9.5	98.1
PS-[V ^V O ₂ (fsal-dmen)]	Benzothiophene	500	8.5	98.3
PS-[V ^V O ₂ (fsal-dmen)]	Dibenzothiophene	500	8	98.4
PS-[V ^V O ₂ (fsal-dmen)]	2-Methylthiophene	500	6	98.8
[V ^{IV} O(fsal-dmen)(acac)]	Thiophene	500	148.5	70.3
[V ^{IV} O(fsal-dmen)(acac)]	Benzothiophene	500	144.5	71.1
[V ^{IV} O(fsal-dmen)(acac)]	Dibenzothiophene	500	141.5	71.7
[V ^{IV} O(fsal-dmen)(acac)]	2-Methylthiophene	500	140.5	71.9
[V ^V O ₂ (fsal-dmen)]	Thiophene	500	113	77.4
[V ^V O ₂ (fsal-dmen)]	Benzothiophene	500	109.5	78.1
[V ^V O ₂ (fsal-dmen)]	Dibenzothiophene	500	111.5	77.7
[V ^V O ₂ (fsal-dmen)]	2-Methylthiophene	500	108	78.4

(11% conversion). All these catalysts are more selective (90%) towards formation of catechol, except [V^{IV}O(sal-1,3-pn)]-Y which only gave ~68% selectivity. The formation of 1,4-benzoquinone was not detected [58]. Similarly catalyst [V^{IV}O-(EtOsaloph)]-Y had 71% conversion after 2 h with selectivity of 92% towards catechol, while [V^{IV}O-(EtOsalnaph)]-Y exhibited 77% conversion after 6 h with almost identical selectivity to catechol (94%) [102].

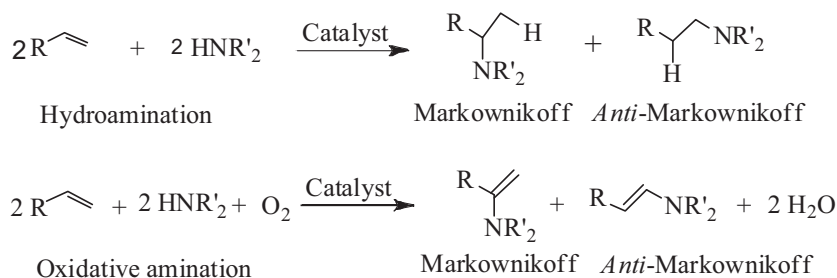
Catalytic action of the V^{IV}O-tetraaza complexes [V^{IV}O(Bzo₂[14]aneN₄)]-Y, [V^{IV}O([14]aneN₄)]-Y, [V^{IV}O(Bzo₂[16]aneN₄)]-Y and [V^{IV}O([16]aneN₄)]-Y for the liquid-phase hydroxylation of phenol with H₂O₂ was between 22 and 38% in CH₃CN, while their selectivity towards catechol is similar to that of NH₄[VO₂(sal-inh)]-Y under similar conditions. [V^{IV}O(N₂X₂)]Y

(X = NH, O) exhibited better conversion with similar product selectivity, but conversion of phenol as well as selectivity of catechol both are low with [V^{IV}O(N₂X₂)]Y (X = S). Some of these complexes have been reused at least twice and they exhibited only minor loss in activity [45,61]. The corresponding N₄-macrocyclic oxovanadium(IV) complexes exhibited slightly lower activity in the oxidation of phenol (20–43%) using H₂O₂ as oxidant. The selectivity of catechol varied between 63 and 79% and was also slightly lower than for the corresponding encapsulated ones. Again, both conversion of phenol as well as selectivity of catechol were low with sulfur containing complexes.

When using H₂O₂ as oxidant vanadium-Pc encapsulated in zeolite-Y (VPc-Y) gave mainly catechol and hydroquinone, and *p*-

Table 4
Oxidation of Phenol and % selectivity of oxidation products: catechol (cat), hydroquinone (Hq) and *p*-benzoquinone (Phq).

Catalyst	% Conv.	TOF (h ⁻¹)	% Selectivity				Reference
			Cat	Hq	Pbq	Others	
[V ^V O ₂ (sal-ambmz)]-Y	44	409	65	35	–	–	[54]
[V ^{IV} O(EtOsaloph)]	72	–	92	8	–	–	[102]
[V ^{IV} O(EtOsalnaph)]	77	–	94	4	–	–	[102]
NH ₄ [V ^V O ₂ (sal-inh)]-Y	27	477	85	15	–	–	[59]
NH ₄ [V ^V O ₂ (sal-oap)]-Y	26	762	77	33	–	–	[59]
[V ^{IV} O(salen)]-Y	33	1940	93	7	–	–	[58]
[V ^{IV} O(sal-1,3-pn)]-Y	34	665	67	32	–	–	[58]
[V ^{IV} O(sal-1,2-pn)]-Y	11	1472	97	3	–	–	[58]
[V ^{IV} O(salten)]-Y	33	1514	92	8	–	–	[58]
[V ^{IV} O(Bzo ₂ [14]aneN ₄)]-Y	38	–	87	13	–	–	[61]
[V ^{IV} O(Bzo ₂ [14]aneN ₄)]-Y ^a	38	–	85	15	–	–	[61]
[V ^{IV} O(Bzo ₂ [14]aneN ₄)]-Y ^c	37	–	84	16	–	–	[61]
[V ^{IV} O([14]aneN ₄)]-Y	33	–	77	23	–	–	[61]
[V ^{IV} O(Bzo ₂ [16]aneN ₄)]-Y	28	–	81	19	–	–	[61]
[V ^{IV} O([16]aneN ₄)]-Y	23	–	73	27	–	–	[61]
[V ^{IV} O([H] ₂ -N ₄)]-Y	50	–	86	14	–	–	[45]
[V ^{IV} O([H] ₂ -N ₄)]-Y ^a	49	77	85	14	–	–	[45]
[V ^{IV} O([H] ₂ -N ₄)]-Y ^b	49	42	84	16	–	–	[45]
[V ^{IV} O([H] ₂ -N ₄)]-Y ^c	48	–	83	17	–	–	[45]
[V ^{IV} O([CH ₃] ₂ -N ₄)]-Y	46	93	73	27	–	–	[45]
[V ^{IV} O([H] ₂ -N ₂ O ₂)]-Y	47	111	75	25	–	–	[45]
[V ^{IV} O([CH ₃] ₂ -N ₂ O ₂)]-Y	45	161	63	37	–	–	[45]
[V ^{IV} O([H] ₂ -N ₂ S ₂)]-Y	37	137	69	31	–	–	[45]
[V ^{IV} O([CH ₃] ₂ -N ₂ S ₂)]-Y	33	–	59	41	–	8	[45]
VPc-Y (1%)	20	–	62	24	6.0	5	[60]
VPc-Y (1.2%)	12	–	53	26	16	–	[60]
Ps-[V ^{IV} O(salten)]	37	–	58	40	2	–	[40]
PS-[V ^{IV} O(sal-ohyba).DMF]	34	–	70	28	–	–	[30]
PS-[V ^V O ₂ (sal-ohyba)]	37	–	67	31	–	–	[30]
PS-K[V ^V O(O ₂) ₂ (2-pybz)]	34	–	62	35	–	–	[39]
PS-K[V ^V O(O ₂) ₂ (3-pybz)]	35	–	62	38	–	–	[39]



Scheme 27. Hydroamination and oxidative amination of olefins producing the Markownikoff- and/or anti-Markownikoff-type products.

benzoquinone (Pbq) as a minor product. The catalytic activity of VPC-Y catalysts decreases with increasing V content from 1.0 to 1.2 wt.%. This decrease was attributed to blockage of pores at higher V contents, as evidenced from the large decrease in surface area [60].

With [V^{IV}O(saldien)] in water/methanol, phenol conversion was only 3% with 100% selectivity towards *p*-benzoquinone. Studying the effect of pH on the conversion of Hq to Phq, using buffers [acetate (pH 4.64), phosphate (pH 6.85) and carbonate (pH 10)], the buffer at pH 10 was the most adequate one, but the conversion was only ~17% [40]. In acetonitrile, the conversion of phenol increased to 37%, but two other products formed [40]. Other polymer-anchored and encapsulated complexes e.g. PS-[V^{IV}O(sal-ohyba)]-DMF, PS-[V^{VO}O₂(sal-ohyba)], PS-K[V^{VO}O(O₂)₂(2/3-pybzsm)] and [V^{VO}O₂(sal-ambmz)]-Y exhibited comparable conversions of 34, 37 and 34%, respectively. These catalysts gave only two main products, catechol and *p*-hydroquinone, with higher selectivity for catechol [30,39,54].

4.4. Hydroamination and oxidative amination

Metal-catalyzed addition of nucleophilic amines to alkenes, called amination, is one of the important routes to synthesize nitrogen containing organic molecules [103]. The amination may proceed in the presence or absence of oxygen and the processes are called oxidative amination or hydroamination, respectively. Both are highly useful and based on regio selectivity, Markownikoff and/or anti-Markownikoff products being produced (Scheme 27).

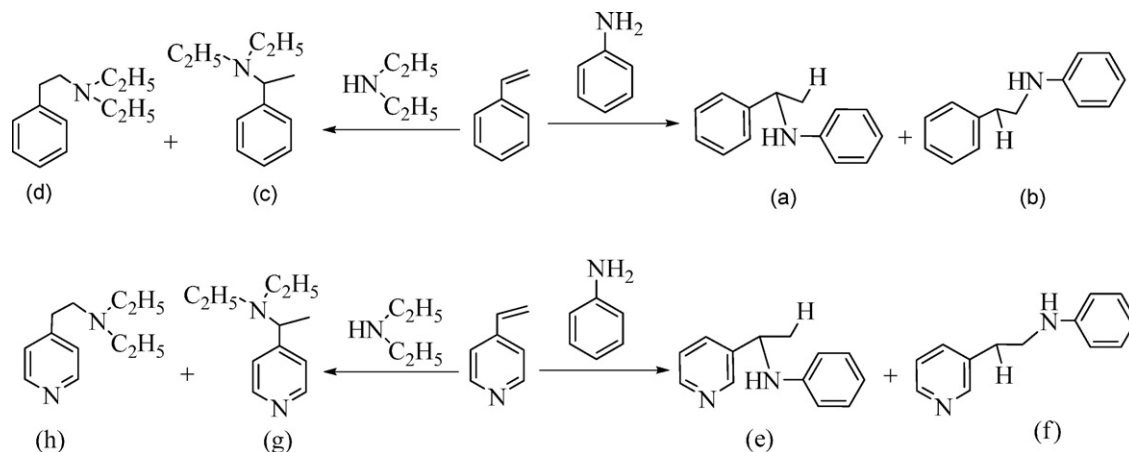
Hydroamination of styrene and vinyl pyridine with amines (aniline and diethylamine) catalyzed by PS-[V^{IV}O(fsal-aepy)](acac) and PS-[V^{VO}O₂(fsal-aepy)] gave the corresponding enamines (Scheme 28) [32].

Table 5 presents data on hydroamination under optimized reaction conditions (previously settled) [32], turn over frequency

(TOF) of the catalyst, and selectivity of the Markownikoff and anti-Markownikoff products obtained. The selectivity for the formation of the anti-Markownikoff products (cf. Scheme 28) are higher than those for the Markownikoff ones, this being explained taking into account the steric hindrance imposed by the amine, which decreases the degree of formation of the Markownikoff products.

The catalytic activity of the neat complex [V^{IV}O(fsal-aepy)](acac) and [V^{VO}O₂(fsal-aepy)], was also tested for the hydroamination of styrene using approximately the same “concentration” as used for PS-[V^{IV}O(fsal-aepy)](acac), and results are also included in Table 5. It is clear from the table that for all reactions the neat complexes exhibit slightly lower conversion than their anchored analogues. The TOFs for all reactions with anchored catalysts are also higher [32]. The improvement in the catalytic activity of the anchored complex may be due to uniform distribution of metal centres on the polymer matrix, and/or an increased availability of styrene molecules which may adsorb on the polymer, close to the catalyst. The recyclability of PS-[V^{IV}O(fsal-aepy)](acac) and PS-[V^{VO}O₂(fsal-aepy)] was checked up to three cycles and the results (Table 5) indicate that these complexes have very good recycle ability [32].

The polymer-anchored complex PS-[V^{IV}O(sal-Cys)](DMF) catalyzes the oxidative amination of styrene with diethylamine, imidazole, and benzimidazole in the presence of oxygen and triethylamine, to give the corresponding enamines (Scheme 29) [29]. Table 6 presents a summary of data. It is clear that again the selectivity for the anti-Markownikoff products (cf. Scheme 29) is higher than those of the Markownikoff compounds. This can be rationalized taking into account the steric hindrance imposed by the secondary amine, which decreases the formation of the Markownikoff products. Within the anti-Markownikoff products the selectivity also follows the order of decreasing steric hindrance.



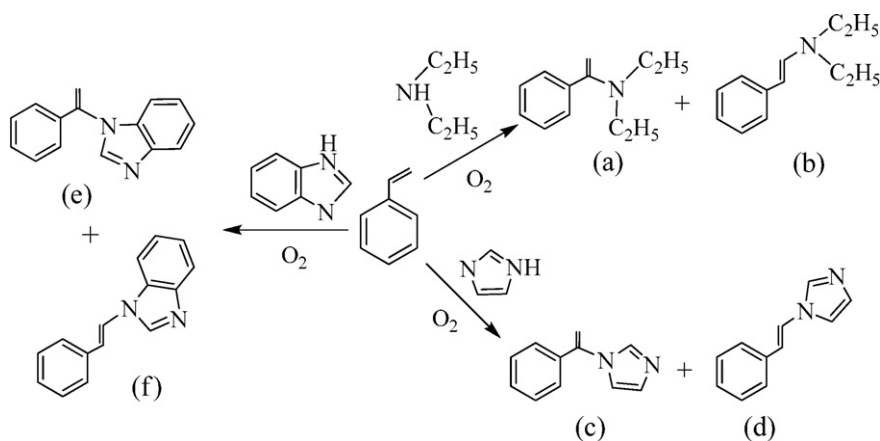
Scheme 28. Products of hydroamination of styrene and vinyl pyridine.

Table 5
Conversion (%) and type of hydroamination products obtained using neat and anchored catalysts [32].

Catalyst	Olefin	Amine	% Conv.	TOF (h ⁻¹)	% Selectivity	
					Markov. product	anti-Markov. product
PS-[V ^{IV} O(fsal-aepy)(acac)]	Styrene	Aniline	66	47	22	78
PS-[V ^{IV} O(fsal-aepy)(acac)] ^a			65	–	22	78
PS-[V ^{IV} O(fsal-aepy)(acac)] ^b		Diethylamine	64	–	21	79
PS-[V ^{IV} O(fsal-aepy)(acac)]			48	34	27	73
PS-[V ^{IV} O(fsal-aepy)(acac)] ^a			47	–	26	74
PS-[V ^{IV} O(fsal-aepy)(acac)] ^b	Vinylpyridine	Aniline	45	–	26	74
PS-[V ^{IV} O(fsal-aepy)(acac)]			82	59	18	82
PS-[V ^{IV} O(fsal-aepy)(acac)] ^a		Diethylamine	82	–	17	83
PS-[V ^{IV} O(fsal-aepy)(acac)] ^b			81	–	16	84
PS-[V ^{IV} O(fsal-aepy)(acac)]			60	43	12	88
PS-[V ^{IV} O(fsal-aepy)(acac)] ^a	Styrene	Aniline	60	–	11	89
PS-[V ^{IV} O(fsal-aepy)(acac)] ^b			59	–	10	90
PS-[V ^V O ₂ (fsal-aepy)]		Diethylamine	76	65	14	86
PS-[V ^V O ₂ (fsal-aepy)] ^a			75	–	14	86
PS-[V ^V O ₂ (fsal-aepy)] ^b			74	–	13	87
PS-[V ^V O ₂ (fsal-aepy)]	Vinylpyridine	Aniline	60	50	29	71
PS-[V ^V O ₂ (fsal-aepy)] ^a			58	–	28	72
PS-[V ^V O ₂ (fsal-aepy)] ^b		Diethylamine	58	–	27	73
PS-[V ^V O ₂ (fsal-aepy)]			92	77	19	81
PS-[V ^V O ₂ (fsal-aepy)] ^a			92	–	18	82
PS-[V ^V O ₂ (fsal-aepy)] ^b	Styrene	Aniline	91	–	18	82
PS-[V ^V O ₂ (fsal-aepy)]			71	59	23	77
PS-[V ^V O ₂ (fsal-aepy)] ^a		Diethylamine	70	–	23	77
PS-[V ^V O ₂ (fsal-aepy)] ^b			69	–	22	78
[V ^{IV} O(fsal-aepy)(acac)]	Vinylpyridine	Aniline	53	21	33	67
[V ^{IV} O(fsal-aepy)(acac)]		Diethylamine	31	12	35	65
[V ^{IV} O(fsal-aepy)(acac)]	Styrene	Aniline	69	27	30	70
[V ^{IV} O(fsal-aepy)(acac)]		Diethylamine	46	36	24	76
[V ^V O ₂ (fsal-aepy)]	Vinylpyridine	Aniline	66	22	26	74
[V ^V O ₂ (fsal-aepy)]		Diethylamine	42	13	34	66
[V ^V O ₂ (fsal-aepy)]	Styrene	Aniline	88	27	32	68
[V ^V O ₂ (fsal-aepy)]		Diethylamine	64	20	25	75

^a First cycle of used catalyst.

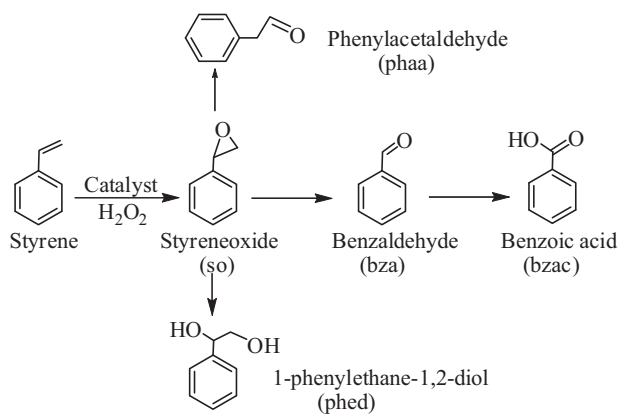
^b Second cycle of used catalyst.



Scheme 29. Oxidative amination using either [V^{IV}O(sal-eta)₂] or PS-[V^{IV}O(sal-Cys)(DMF)] (**15**) as catalyst precursors.

Table 6
Conversion and reaction products of the oxidative amination of styrene using neat [V^VO(sal-eta)₂] and anchored PS-[V^{IV}O(sal-Cys)(DMF)] catalysts [29].

Catalyst	Substrate	% Conversion	TOF (h ⁻¹)	Products/% selectivity	
				Markownikoff	anti-Markownikoff
PS-[V ^{IV} O(fsal-Cys)(DMF)]	Diethylamine	73	39	29	71
PS-[V ^{IV} O(fsal-Cys)(DMF)]	Imidazole	56	30	26	74
PS-[V ^{IV} O(fsal-Cys)(DMF)]	Benzimidazole	24	13	19	81
[V ^{IV} O(sal-eta) ₂]	Diethylamine	65	21	33	67
[V ^{IV} O(sal-eta) ₂]	Imidazole	47	14	27	73
[V ^{IV} O(sal-eta) ₂]	Benzimidazole	21	7	21	79



Scheme 30. Products of oxidation of styrene.

4.5. Oxidation of styrene

Catalytic oxidation of styrene using a mild oxidant such as TBHP normally gives styrene oxide, while a stronger oxidant may give rise to several other products. The formation of at least five products (Scheme 30) was observed when PS-[V^{IV}O(sal-ohyba)(DMF)], PS-K[V^VO(O₂)(2-pybmz)] and PS-K[V^VO(O₂)(3-pybmz)] were applied as catalysts [30,39]. The zeolite-Y encapsulated complexes e.g. [V^VO₂(sal-ambmz)]-Y, [V^VO₂(sal-oaba)H₂O]-Y and [V^{IV}O(sal-dach)]-Y have also shown similar results [54–57]. Table 7 presents conversion and selectivity data for several of the catalyst precursors used.

Table 7
Conversion of styrene, product selectivity and TOF^a.

Catalyst	% Conv.	TOF (h ⁻¹)	% Selectivity ^b					
			so	phaa	bza	bzac	phed	Others
PS-K[V ^V O ₂ (fsal-ohyba)]	8	30	3.5	3.0	60.7	9.8	20.6	2.4
PS-[V ^{IV} O(fsal-ohyba)(DMF)]	73	25	3.2	4.2	60.7	8.5	18.8	4.6
[V ^{IV} O(fsal-ohyba)]	57	8	4.3	5.4	53.4	11.5	21.2	4.2
[K(H ₂ O)][V ^V O ₂ (fsal-ohyba)]	64	11	3.8	4.2	57.3	9.6	20.5	4.6
[V ^{IV} O(sal-ohyba)]	53	7	3.9	3.8	58.2	9.9	19.9	4.3
[K(H ₂ O)][V ^V O ₂ (sal-ohyba)]	61	11	3.2	3.9	57.6	10.8	20.3	4.2
PS-[V ^{IV} O(fsal-β-Ala)(DMF)]	46	20	15.3	–	75.5	3.2	5.7	–
PS-[V ^{IV} O(fsal-ea)(DMF)]	90	23	4.1	2.9	58.4	7.6	23.5	3.5
PS-[V ^{IV} O(fsal-pa)(DMF)]	95	26	3.8	3.5	62.8	8.7	17.3	3.8
PS-[V ^{IV} O(fsal-amp)(DMF)]	82	24	4.3	3.9	60.6	9.0	18.3	4.0
[V ^{IV} O(fsal-ea)] ₂	65	15	3.9	3.1	61.7	18.3	8.8	4.3
[V ^{IV} O(fsal-pa)] ₂	70	16	3.6	3.8	62.5	17.2	8.8	4.2
[V ^{IV} O(fsal-amp)] ₂	62	18	3.9	3.4	60.4	18.8	8.9	4.6
PS-[V ^{IV} O(hpbmz) ₂]	71	61	5.2	1.1	72.2	5.8	15.7	–
[V ^{IV} O(hpbmz) ₂]	52	8	3.0	1.4	82.4	3.1	10.1	–
PS-[V ^{IV} O(hmbmz) ₂]	48	–	4.4	–	78.6	–	–	17.0
[V ^{IV} O(hmbmz) ₂]	4	–	–	–	75.0	–	–	25.0
PS-[V ^{IV} O(ligand) _n]	81	38	4.9	–	62.6	–	31.3	1.2
PS-[V ^{IV} O(ligand) _n] ^c	80	–	3.8	2.0	62.5	6.9	31.6	1.1
PS-[V ^{IV} O(ligand) _n] ^d	80	–	3.6	1.7	62.7	3.8	31.5	1.2
[V ^{IV} O(tmbmz) ₂]	65	22	3.6	2.3	66.3	9.6	28.6	1.5
PS-K[V ^V O(O ₂)(2-pybmz)]	73	35	2.9	0.2	65.7	13.2	19.7	2.8
PS-K[V ^V O(O ₂)(3-pybmz)]	63	24	4.8	2.1	64.6	6.7	23.1	2.0
[V ^{IV} O(tmbmz) ₂]-Y	96	205	6.1	4.9	68.1	8.9	12.4	1.5
[V ^V O ₂ (sal-ambmz)]-Y	97	151	5.4	–	54.9	–	25.3	1.0
[V ^V O ₂ (sal-oaba)H ₂ O]-Y	89	696	6.8	–	58.8	–	24.1	1.5
[V ^{IV} O(sal-dach)]-Y	95	328	7.6	–	54.2	–	22.5	1.9
[V ^{IV} O(saldien)]-Y	35	2362	35.5	–	11.5	–	–	53.0
[V ^{IV} O(saldien)]-Y ^c	30	–	27.6	–	13.8	–	–	58.6
[V ^{IV} O(saldien)]-MCM-41	41	2753	45.0	–	7.7	–	–	47.3
[V ^{IV} O(saldien)]-MCM-41 ^c	29	–	37.2	–	7.5	–	–	55.3

^a Refer to text for references concerning catalysts.

^b The nature of “ligand” is discussed when introducing Scheme 30.

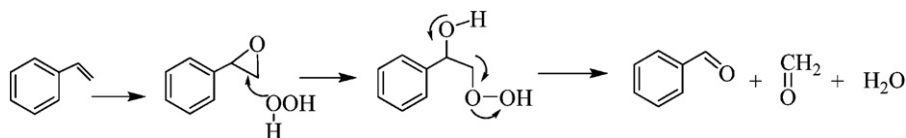
^c First cycle of used catalyst.

^d Second cycle of used catalyst.

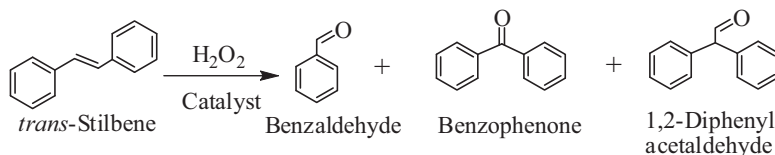
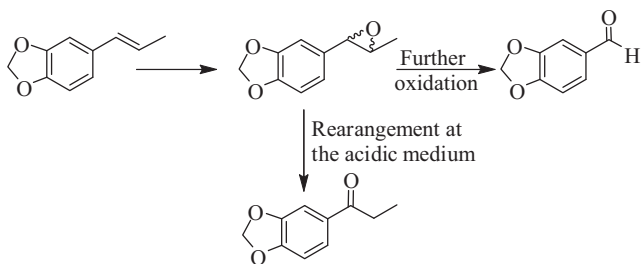
Among all products (Table 7), the formation of benzaldehyde in highest yield is possibly due to the conversion of most of the styrene oxide initially formed to benzaldehyde, via nucleophilic attack of H₂O₂ to styrene oxide followed by the cleavage of the intermediate hydroperoxystyrene (Scheme 31). Benzaldehyde formation may also occur by direct oxidative cleavage of the styrene side chain double bond via radical mechanism [104]. Benzoic acid may form through benzaldehyde, but this is normally a slow process. The formation of phenylacetaldehyde, a product that may form by isomerisation of styrene oxide, is either very low or not observed. Water used as solvent for H₂O₂ is probably responsible for the hydrolysis of styrene oxide to 1-phenylethane-1,2-diol.

4.6. Oxidation of *trans*-stilbene, isosafrol and geraniol

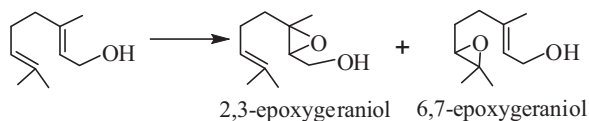
In the oxidation of *trans*-stilbene catalyzed by e.g. PS-[V^{IV}O(fsal-β-Ala)(DMF)] in the presence of H₂O₂, only ca. 16% conversion was achieved after 6 h. The oxidation products obtained were benzaldehyde (ca. 13%), 1,2-diphenyl acetaldehyde (ca. 2%), and benzophenone (ca. 1%) (Scheme 32). No epoxide was detected among the reaction products and this suggested that the intermediate epoxide formed, if any, was further oxidized to give other products [34]. The neat complex [V^{IV}O(saloph)] is not a good catalyst precursor for the oxidation of *trans*-stilbene (only 9% conversion with 73 wt% selectivity for the epoxide) but with zeolite-Y encapsulated or MCM grafted versions, conversion was ~37 and 48%, respectively, with selectivity towards epoxide of 85% ([V^{IV}O(saloph)]-Y) and 89% ([V^{IV}O(saloph)]-MCM-41). The recycled catalysts also exhibited similar conversion and selectivity [51,64]. EPR spectroscopic studies suggested the oxido-bridged dimerisa-



Scheme 31.

Scheme 32. Reaction products of oxidation of *trans*-stilbene.

Scheme 33.



Scheme 34.

tion of neat complex in the presence of oxidant to be responsible for the deactivation of catalyst and poor activity.

[VO(salen)] encapsulated in zeolite-Y as well as impregnated on Na-Y were used for the oxidation of isosafrol (1,2-methylenedioxy-4(1-propenyl)benzene; Scheme 33) under microwave. VO(salen)-Y gave 67% conversion where selectivity of epoxide (c) was 79% while that of the rearranged product (d) was 19%. Though conversion by impregnate sample was low (51%), the selectivity of epoxide increased to 90%. Catalyst's surface area and availability of the vanadyl group were the main factors which allowed this superior performance [105].

Hexagonal mesoporous silica (HMS) grafted [V^{IV}O(acac)₂] was used as catalyst for the epoxidation of geraniol using TBHP as oxygen source [74,75]. Though geraniol always resulted in 2,3-epoxygeraniol and 6,7-epoxygeraniol (Scheme 34), the selectivity of the former one was always higher while conversion varied with the nature of grafting method of [V^{IV}O(acac)₂]. In general, the fresh catalyst gave poor conversion while the recycled one improved their efficiency considerably. The catalyst prepared by functionalization of the HMS with 3-aminopropyltriethoxysilane (APTES) followed by complex immobilization allowed higher substrate con-

version but it leaches during catalytic reaction. This leaching is lower for the catalyst where the unreacted surface silanol groups were deactivated with trimethylethoxysilane (TMS).

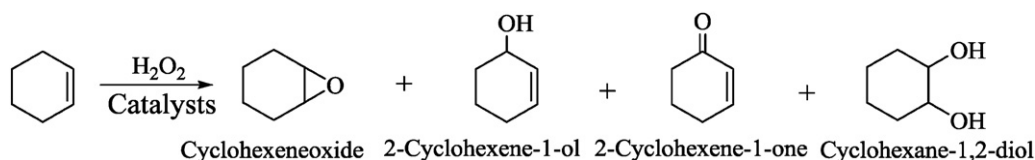
4.7. Oxidation of cyclohexene, cyclooctene and limonene

Oxidation of cyclohexene catalyzed by polymer-anchored complexes (e.g. PS-[V^{IV}O(fsar-DL-Ala)(H₂O)], PS-[V^{IV}O(fsar-L-Ile)(H₂O)] [35], PS-[V^{IV}O(fsar-β-Ala)(DMF)] [34]) and zeolite-Y encapsulated complexes (e.g. [V^{IV}O(sal-dach)]-Y [55]) gave up to four oxidized products, which are specified in Scheme 35. Complexes [V^{IV}O(dipy)₂]²⁺-Y and [V^{IV}O(salen)]-Y are selective for the formation of cyclohexene epoxide. The much improved activity and selectivity of [V^{IV}O(salen)]-Y as compared to neat [V^{IV}O(salen)] was attributed to the site-isolation effect i.e. the non-formation of the inactive μ-oxido-dinuclear complexes [49]. The [V^{IV}O(dipy)₂]²⁺ could be reused without any loss of activity or selectivity [62].

Table 8 presents the conversions of cyclohexene after 6 h along with the product selectivity. Neat complexes exhibit lower conversion along with lower TOFs, but the selectivity for the major products follows the same trends as for their heterogenized versions. The PS-anchored catalysts did not leach during the catalytic reactions and were recyclable up to at least three cycles without much loss in activity. The recovered PS-anchored as well as encapsulated V^{IV}O catalysts exhibit similar IR, electronic and EPR spectral patterns, suggesting that their original state is maintained after their recovery, these catalysts thus being recyclable.

The formation of the allylic oxidation products 2-cyclohexene-1-one and 2-cyclohexene-1-ol reflects the preferential attack of the activated C–H bond over the C=C bond [106]. Valentine and co-workers [107] suggested that the species responsible for the cyclohexene oxidation is the product formed from the cleavage of the O–O bond, whereas epoxidation occurs via the direct reaction of the olefin with the coordinated HOO[−]. Since the O–O bond of HOOH is 5 kcal mol^{−1} (21 kJ mol^{−1}) stronger than TBHP, an HOO[−] complex is expected to have higher activation energy for O–O bond cleavage than the corresponding TBHP complex and therefore, will have a longer lifetime and a higher probability of forming the epoxide.

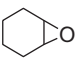
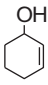
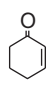
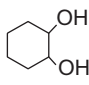
[VO(acac)]Ph-DAB-(CH₂)₃Si(OEt)₃ (52, Scheme 23(A)) was bound to MCM-41 by two different methods, grafting and tethering, with lower vanadium loading for the grafted catalyst, but

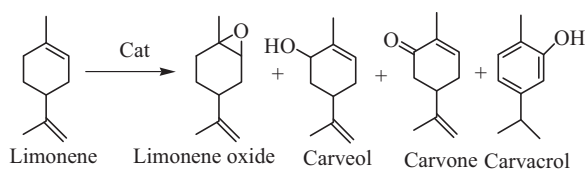


Scheme 35. Oxidation products of cyclohexene.

Table 8

Conversion of cyclohexene and selectivity of various oxidation products after 6 h of reaction time.

Catalyst	% Conv.	TOF (h ⁻¹)	% Selectivity				Reference
							
PS-[V ^{IV} O(fsal-DL-Ala)(H ₂ O)]	79	50	34.7	48.1	6.8	10.4	[35]
PS-[V ^{IV} O(fsal-DL-Ala)(H ₂ O)] ^a	78	–	34.6	48.3	6.7	10.4	[35]
[V ^{IV} O(fsal-DL-Ala)(H ₂ O)]	54	34	38.9	52.6	5.1	3.4	[35]
PS-[V ^{IV} O(fsal-L-Ile)(H ₂ O)]	77	57	36.1	44.7	8.2	11.0	[35]
PS-[V ^{IV} O(fsal-L-Ile)(H ₂ O)] ^a	76	–	36.3	44.6	8.2	10.9	[35]
[V ^{IV} O(fsal-L-Ile)(H ₂ O)]	51	38	40.0	48.4	6.3	5.28	[35]
PS-[V ^{IV} O(fsal-β-Ala)(H ₂ O)]	36	16	9.0	50.0	41.0	–	[34]
PS-[V ^{IV} O(ligand) _n]	86	31	3.2	–	14.8	81.3	[43]
PS-[V ^{IV} O(ligand) _n] ^a	86	–	3.0	–	14.9	81.2	[43]
PS-[V ^{IV} O(ligand) _n] ^b	85	–	3.1	–	14.8	81.2	[43]
[V ^{IV} O(tmbmz) ₂]	64	15	2.4	–	12.4	84.7	[43]

^a First cycle of used catalyst.^b Second cycle of used catalyst.**Scheme 36.**

the grafted material was more stable towards metal leaching. Both of them were tested as catalysts in the epoxidation of cyclooctene with TBHP at 328 K. After 24 h of reaction, 1,2-epoxycyclooctane was the main product (ca. 98% selectivity) with conversions of 61 and 83% at 24 h reaction. The initial TOF was practically the same for both (148 and 150 h⁻¹) but after ca. 15 min, the reaction becomes faster in the case of the tethered catalyst, most likely due to its higher metal loading. Upon recovering the catalysts, partial loss of catalytic activity in consecutive reaction runs was observed for tethered and grafted materials, suggesting that deactivation phenomena are involved, possibly changes in the nature of the surface metal species [63].

[V^{IV}O(salten)] grafted in SBA-15 (**46**, Scheme 19) was used for the oxyfunctionalization of limonene with UHP as the oxidizing agent. With a conversion of ca. 20%, the products obtained were: limonene oxide (33%), carvone (23%), carvacrol (15%) and carveol (18%) along with an unidentified product (8.0%) (Scheme 36). The corresponding neat complex exhibited only ca. 5% oxidation with similar selectivity, but deactivated in the reaction mixture due to the formation of inactive α-oxo-bridged dinuclear species, as indicated by spectroscopic studies. The anchored complexes remained stable throughout the reaction, and the catalyst could be easily separated from the products and reused after washing and drying. In the absence of the catalyst no allylic oxidation products were detected [64].

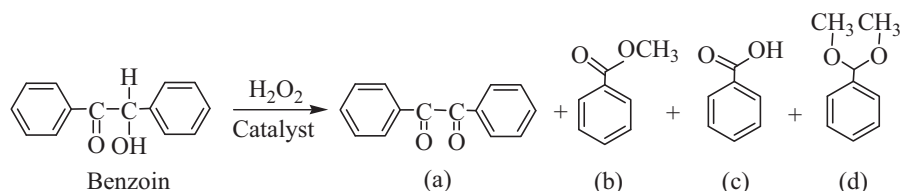
An organic–inorganic hybrid heterogeneous catalyst (V-MCM-41) was synthesized by anchoring [V^{IV}O(salten)] on chloropropyl

modified mesoporous silica (CP-MCM-41). Epoxidations of various olefins using V-MCM-41 as the catalyst precursor, H₂O₂ as the oxidant and sodium bicarbonate as the co-catalyst in acetonitrile were carried out for several olefins: cyclohexene, styrene, norbornene, allylic alcohol, 1-octene, cyclooctene and crotyl alcohol. The catalytic efficiency of H₂O₂ when it is used as sole oxidant is often rather poor as compared to H₂O₂ and peracids in epoxidation. However, the use of NaHCO₃ as co-catalyst enhanced the rate of reaction by many folds, giving conversions of 82–95% with selectivity for the epoxide of ca. 90–98% [66]. The reaction requires minimum amount of H₂O₂, short time period and proceeds at room temperature. The heterogeneous catalyst could be recovered easily and reused many times without significant loss in catalytic activity and selectivity.

4.8. Oxidation of benzoin

The oxidation of benzoin was successfully achieved with the catalyst precursors PS-[V^{IV}O(sal-his)(acac)], PS-[V^VO₂(sal-his)] and PS-[V^{IV}O(hebmz)₂]. The main products obtained are indicated in Scheme 37.

Under “optimized conditions” using PS-[V^VO₂(sal-his)] (**13**, Scheme 10) in methanol as catalyst precursor, at the first stage of the reaction the selectivity was highest for benzil (ca. 50%), but with time a continuous slow decrease of the selectivity for this product was observed, which finally reached 31% after 6 h. During the same period the selectivity for benzoic acid and benzaldehyde-dimethylacetal increased only marginally, while that for methyl benzoate increased considerably from 15 to 37%. After 6 h 91% of benzoin oxidized and the final selectivity profile was: methyl benzoate (37%) > benzil (31%) > benzaldehyde-dimethylacetal (22%) > benzoic acid (8%). The corresponding neat complex gave ca. 76% conversion. The catalytic activity of PS-[V^{IV}O(sal-his)(acac)] (**12**, Scheme 10) was also good, yielding ca. 83% conversion of benzoin, while [V^VO₂(sal-his)] gave ca. 71%, the selectivity for the different products being nearly the same under similar reaction conditions [41].

**Scheme 37.** Oxidized products of benzoin: (a) benzil, (b) methyl benzoate, (c) benzoic acid and (d) benzaldehyde-dimethylacetal.

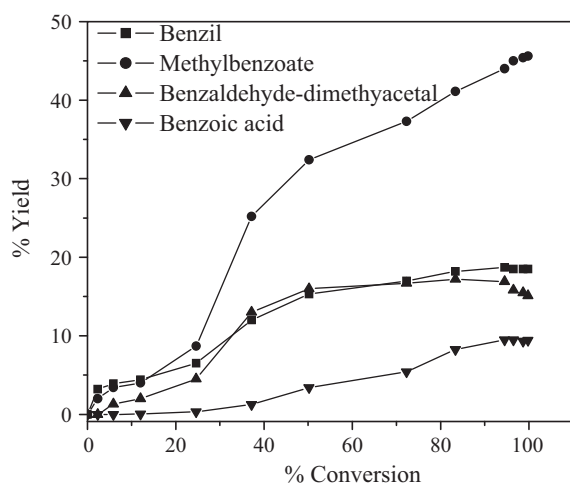


Fig. 3. Formation different products versus conversion of benzoin by oxidation with TBHP. The reaction was carried out under “optimized conditions”: benzoin (5 mmol), 70% TBHP (2.754 g, 20 mmol), PS-[V^{IV}O(hebzmz)₂] (0.030 g, 0.012 mmol) and methanol (25 mL).

Fig. 3 depicts the % formation of the various reaction products as a function of conversion of benzoin during 6 h of reaction time upon using PS-[V^{IV}O(hebzmz)₂] as catalyst precursor and TBHP as oxidizing agent, in methanol. After ca. 6 h of reaction, 99.8% of benzoin had oxidized, and the percent yield of reaction products varied in the order: methylbenzoate (46%) > benzil (18%) > benzaldehyde-dimethylacetal (15%) > benzoic acid (10%) [83]. Other unidentified products formed in small amounts were ignored.

To obtain evidence for the intermediate species formed during the catalytic reaction PS-[V^{IV}O(hebzmz)₂] was treated with benzoin (slight excess than molar equivalent) in methanol and the EPR spectrum of the mixture recorded at 130 K was compared with that of pure PS-[V^{IV}O(hebzmz)₂]. The mixture showed an additional EPR signal (indicated by an arrow in **Fig. 4(b)**) corresponding to a slightly higher $A_{||}$ value than that observed in (b), for pure polymer-anchored complex. Addition of TBHP to PS-[V^{IV}O(hebzmz)₂] in methanol resulted in the reduction of EPR signals considerably (an expanded EPR signal is depicted in **Fig. 4(c)**) suggesting the oxidation of most of the V(IV) initially present. An EPR-silent species was obtained upon addition of TBHP and benzoin to PS-[V^{IV}O(hebzmz)₂] in methanol (**Fig. 4(d)**). Similar results were obtained with neat [V^{IV}O(hebzmz)₂].

4.9. Oxidation of cyclohexane

Oxidation of cyclohexane catalyzed by zeolite-Y encapsulated complexes [V^{IV}O(sal-dach)]-Y and [V^{IV}O(sal-oaba)(H₂O)]-Y was reported by Maurya et al. [55,56]. Upon 21% conversion in 2 h in CH₃CN at 70 °C the products were cyclohexanone, cyclohexanol and cyclohexane-1,2-diol (**Scheme 38**), along with an unknown product. The selectivity for cyclohexanol was ca. 93%.

With [V^{IV}O(sal-oaba)(H₂O)]-Y as catalyst precursor, only 15% conversion was achieved and the selectivity of two major products were: cyclohexanone (57%) and cyclohexanol (38%). The non-identified product (ca. 5%) can either be cyclohexane-1,2-diol or cyclohexyl hydroperoxide. [56]. Knops-Gerrits et al. observed the formation of cyclohexylhydroperoxide during the catalytic oxidation of cyclohexane by [V^{IV}O(bipy)₂]²⁺-Y, as well as cyclohexanol and cyclohexanone, which probably are the result of cyclohexylhydroperoxide decomposition [62]. Kozlov et al. also made similar observations while using [V^{IV}O(pic)₂]-Y, but this catalyst progressively leached from the support [86].

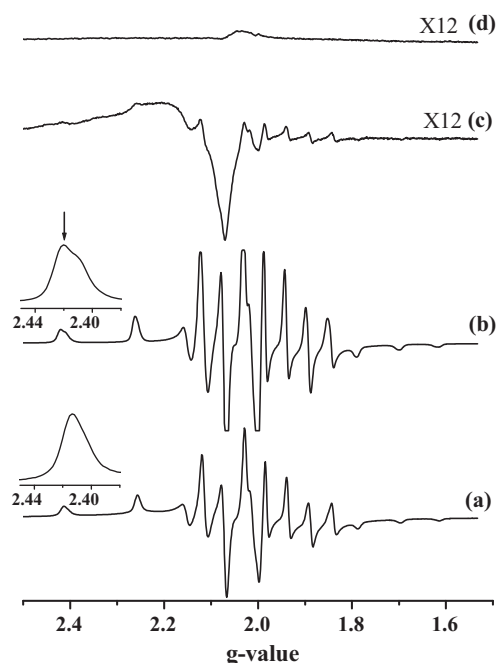
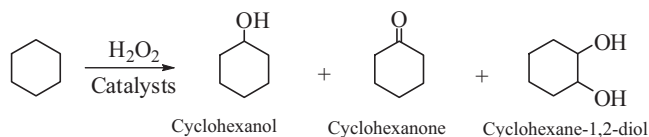


Fig. 4. First derivative EPR spectra measured at 130 K. (a) PS-[V^{IV}O(hebzmz)₂], (b) PS-[V^{IV}O(hebzmz)₂] + benzoin + methanol, (c) PS [V^{IV}O(hebzmz)₂] + TBHP in methanol and (d) PS-[V^{IV}O(hebzmz)₂] + TBHP + benzoin + methanol. The components at higher g values are shown in an expanded form in (a) and (b). The additional peak in part (b) is indicated by an arrow.



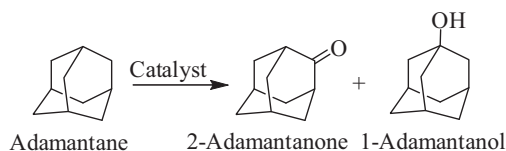
Scheme 38. Products of oxidation of cyclohexane [55,56].

4.10. Oxidation of adamantane

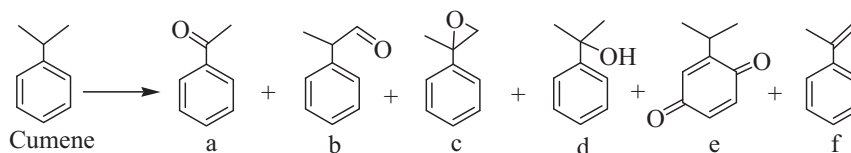
[V^{IV}O(salten)] was bound to MCM-41 through a covalently linked organic spacer and used for the catalytic oxidation of adamantane using UHP as the oxidizing agent at 60 °C (**Scheme 39**). The use of UHP significantly improved the oxidation of adamantane as compared to aqueous H₂O₂. This was ascribed to the slow release of peroxide from the urea-hydroperoxide adduct. No leaching of the complex was observed. The conversion was low in the case of the corresponding homogeneous complex as compared to that of immobilized complex, this being ascribed to the formation of the inactive μ -oxo-bridged species when using the “neat” [V^{IV}O(salten)] [65].

4.11. Oxidation of benzene, naphthalene, cumene, p-chlorotoluene and ethylbenzene

Aromatic C–H oxidation is one of the most challenging problems in organic synthesis. The aromatic nucleus is resistant to



Scheme 39. Products of oxidation of adamantane.



Scheme 40. a = acetophenone, b = 2-phenylpropanal, c = α -methylstyrene epoxide, d = 2-phenyl-2-propanol, e = 2-isopropyl-1,4-benzoquinone and f = α -methylstyrene.

oxidation because of its resonance stabilization, therefore oxygenation almost invariably requires a highly reactive oxidant under severe conditions [108]. Vanadium based catalytic systems have been successfully used for this purpose. Oxidation of benzene gave phenol as the main product. Small amounts of hydroquinone and benzoquinone were also obtained due to subsequent oxidation of phenol. Thus, under “optimized conditions”; in CH_3CN at 75°C , $\text{PS-[V}^{\text{IV}}\text{O(fsal-}\beta\text{-ala)}\text{]}(\text{DMF})$ gave ca. 39% conversion and all three products were obtained with the selectivity order: phenol (94%) > hydroquinone (5%) and benzoquinone (1%) [34]. This catalyst precursor was also used under similar conditions for the oxidation of cumene and naphthalene, and conversions of 20 and 11% were obtained, respectively. Around 15% conversion of benzene with $\text{PS-K[V}^{\text{V}}\text{O}_2(\text{sal-inh})(\text{im})]$ and $[\text{PS-K[V}^{\text{V}}\text{O}_2(\text{sal-bhz})(\text{im})]$ with selectivity of ca. 94% towards phenol was also achieved [44]. All these catalysts could be reused but with slight loss in activity.

The surface functionalization of MCM-41 with amino groups followed by reaction with $\text{V}^{\text{IV}}\text{O}^{2+}$ and calcinations at 540°C for 8 h provided V-MCM-41 materials. These catalysts, of variable loadings, hydroxylate benzene using 30% H_2O_2 , with conversions as high as 59%. The use of TBHP yielded lower conversion [67].

Oxidation of cumene by polymer-anchored complexes $\text{PS-[V}^{\text{IV}}\text{O(fsal-ea)}\text{]}(\text{DMF})$, $\text{PS-[V}^{\text{IV}}\text{O(fsal-pa)}\text{]}(\text{DMF})$ and $\text{PS-[V}^{\text{IV}}\text{O(fsal-amp)}\text{]}(\text{DMF})$ gave the products depicted in Scheme 40. Under “optimized conditions” in acetonitrile at 80°C , the conversions of cumene after 6 h were: $\text{PS-[V}^{\text{IV}}\text{O(fsal-pa)}\text{]}(\text{DMF})$ (41%) > $\text{PS-[V}^{\text{IV}}\text{O(fsal-ea)}\text{]}(\text{DMF})$ (39%) > $\text{PS-[V}^{\text{IV}}\text{O(fsal-amp)}\text{]}(\text{DMF})$ (35%). Independently of catalyst the selectivity of products was: acetophenone > 2-phenyl-2-propanol > α -methylstyrene epoxide > 2-phenylpropanol > 2-isopropyl-1,4-benzoquinone \approx α -methylstyrene [31].

The oxidation of *p*-chlorotoluene was achieved using the catalyst precursors $\text{PS-[V}^{\text{IV}}\text{O(fsal-DL-Ala)}\text{]}(\text{H}_2\text{O})$, $\text{PS-[V}^{\text{IV}}\text{O(fsal-L-Ile)}\text{]}(\text{H}_2\text{O})$ with H_2O_2 as the oxidant. Under the “optimized conditions” in CH_3CN at 80°C , the maximum conversion was ca. 14% with the main products in the order: *p*-chlorobenzaldehyde \gg *p*-chlorobenzylalcohol > *p*-chlorobenzoic acid > 2-methyl-5-chlorophenol > 3-methyl-6-chlorophenol. The catalysts used, were washed with acetonitrile, dried and tested again, the data showing that there was not much loss in catalytic activity. The corresponding non-polymer-bound complexes exhibited lower conversions as well as lower turn-over frequencies [35].

Acetophenone is an important compound in industry due to its use as an intermediate in pharmaceuticals, resins, alcohols, esters, aldehydes, and tear gas. Oxidation of ethylbenzene with a

mild oxidant usually yields acetophenone as the major product, while strong oxidants give several oxidized products. The polymer-anchored vanadium complexes $\text{PS-[V}^{\text{IV}}\text{O(sal-ohya)}\text{]}(\text{DMF})$, $\text{PS-K[V}^{\text{V}}\text{O}_2(\text{fsal-ohya})]$ and $\text{PS-[V}^{\text{IV}}\text{O(hpbmz)}_2]$ were used as catalyst precursors for this purpose using H_2O_2 , but yielded the products indicated in Scheme 41 [30,37]. Table 9 presents the results under the “optimized conditions” established for maximum conversion of ethylbenzene oxidation. Using TBHP and $\text{PS-[V}^{\text{IV}}\text{O(hmbmz)}_2]$ as catalyst precursor acetophenone was obtained selectively but the overall conversion was only ca. 2.5% [82].

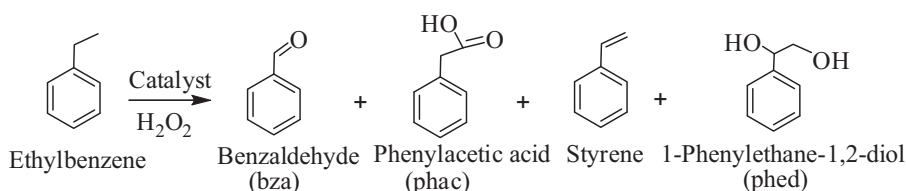
$\text{PS-[V}^{\text{IV}}\text{O(ligand)}_n]$ (**17**) catalyzed the oxidation, by aqueous 30% H_2O_2 , of ethylbenzene to give acetophenone, benzaldehyde, phenyl acetic acid and 1-phenylethane-1,2-diol. The conversion obtained of ca. 25% being ca. 50% higher than that with the corresponding neat complex $[\text{V}^{\text{IV}}\text{O(tmbmz)}_2]$. Additionally there was almost no loss in activity after 3 cycles of their use [43].

4.12. Oxidation of alkanes

$[\text{V}^{\text{IV}}\text{O(pic)}_2]$, $[\text{V}^{\text{IV}}\text{O(sal)}_2]$, $[\text{V}^{\text{IV}}\text{O(salen)}]$ and $[\text{V}^{\text{IV}}\text{O(MeOsalen)}]$ were encapsulated and adsorbed to prepare encapsulated and adsorbed catalyst [50]. The encapsulated complexes showed activity in the selective oxidation of hydrocarbons with H_2O_2 and TBHP, and regioselective oxidation of *n*-hexane, *n*-octane and 2,5-dimethylhexane was studied by using $[\text{V}^{\text{IV}}\text{O(pic)}_2]\text{-Y}$ [86]. The catalytic performance of the encapsulated complex was also compared with that of corresponding homogeneous catalyst $\text{H[V}^{\text{V}}\text{O(O}_2\text{)(pic)}_2]\text{-H}_2\text{O}$ [50,86]. The $[\text{V}^{\text{IV}}\text{O(pic)}_2]\text{-Y}$ retains solution-like activity in aliphatic and aromatic hydrocarbon oxidations as well as in alcohol oxidation. In addition, this encapsulated catalyst showed a number of distinct features such as preferable oxidation of smaller substrates in competitive oxidations, increased selectivity for the oxidation of the terminal CH_3 group in isomeric octanes and preferable, sometimes exclusive, formation of alkyl hydroperoxides in alkane oxidations. These distinct features were explained in terms of intrazeolitic location of the active complexes that imposed transport discrimination and substrate orientation, thus yielding regioselective hydroxylations [86].

4.13. Oxidation of α -hydroxy esters

Chiral α -hydroxy esters are of significant interest as these compounds are useful building blocks for chiral syntheses in the pharmaceutical and fine chemical industries, and extensive research has been dedicated to develop catalytic systems to obtain chiral pure α -hydroxy esters and other secondary alcohols. An



Scheme 41. Reaction products on oxidation of ethylbenzene.

Table 9

Effect of oxidant on conversion of ethylbenzene and selectivity of various oxidation products (see Scheme 40) after 6 h of reaction.

Catalyst	% Conv.	TOF(h ⁻¹)	% Selectivity ^a						Reference
			aph	phac	bza	Styrene	Phed	Others	
PS-K[V ^{IV} O ₂ (fsal-ohyba)]	40	5	–	8	88	2	–	2	[30]
PS-[V ^{IV} O(fsal-ohyba)] DMF	37	4	–	8	85	5	–	2	[30]
PS-[V ^{IV} O(hpbmz) ₂]	31	29	–	8	72	2	16	2	[37]
PS-[V ^{IV} O(ligand) _n]	26	6	6	23	67	–	4	–	[43]
PS-[V ^{IV} O(ligand) _n] ^b	25	–	6	23	67	–	4	–	[43]
PS-[V ^{IV} O(ligand) _n] ^c	24	–	6	23	67	–	4	–	[43]

^a aph: acetophenone, phac: phenylacetic acid, bza: benzoic acid, phed: 1-phenylethane-1,2-diol.^b First cycle of used catalyst PS-[VO(ligand)_n].^c Second cycle of used catalyst.

important subset of these systems exploit the kinetic resolution of racemic substrates and tridentate Schiff base vanadium catalysts derived from salicylaldehyde and *t*-leucinol or *t*-leucine have been shown to promote the oxidative kinetic resolution of racemic α -hydroxy esters by the selective oxidation of only one enantiomer [109–111]. This reaction is attractive not only due to the high enantioselectivity obtained but also due to the use of O₂ at atmospheric pressure as the primary oxidant.

The corresponding semi-soluble and insoluble catalysts were also synthesized and characterized [112]. Linear polystyrene supported catalysts are partially soluble under the reaction conditions used and the soluble species contribute significantly to the catalytic reactivity. The corresponding insoluble catalysts supported on cross-linked polystyrene and mesoporous silica were also prepared. These allowed catalyst recovery and recycling, showing equivalent selectivity over multiple reaction cycles. The mesoporous silica SBA-15 supported catalyst exhibited greater selectivity than the analogous homogeneous and PS-supported catalysts. Interestingly, although some results indicate that the activity and selectivity was maintained for at least four cycles, more rigorous recycle studies showed a loss of activity in each recycle, which was attributed to the cleavage of the imine functionality in the ligand and consequent decomposition of the complex [112].

4.14. Formation of cyanohydrins

A series of chiral V^{IV}O(salen) complexes having a terminal carbon–carbon double bond pendent alkyl chains of various lengths attached to the *para* position of the salen ligand were prepared and anchored on three large surface area silicas, namely amorphous silica, ITQ-2, and MCM-41 through mercaptopropylsilyl groups [69]. The resulting solids, with vanadium loadings of ca. 0.04 mmol/g were tested as enantioselective catalysts for the reaction of aldehyde with trimethylsilyl cyanide. Low ee values compared to solution were found, and to optimize the enantioselectivity of the solid catalysts, silylation of the free silanol groups, variation of the linker length, and screening of the solvent were studied. The optimized enantioselective catalyst was that in which the [V^{IV}O(salen)] is anchored to amorphous silica with the longest alkyl chain of the series (11 C) and in which the residual Si–OH groups were deactivated with trimethylsilyl moieties. Under optimal conditions, the use of CHCl₃ as solvent and at 0 °C, the activity of these solid catalysts is very close to that of the analogous complexes in solution. The solid catalyst can be reused by simple filtration up to three times, retaining a large part of the activity of the fresh catalyst [69].

This study is an interesting example elucidating that anchoring of a highly enantioselective complex on a solid surface may reduce its asymmetric induction capability, due to its interaction with the solid surface, but it is possible to increase the enantioselectivity of the anchored complex to the values obtained in solution. The use

of an adequate spacer linking the complex and the solid, allowing the complex to have a large conformational freedom, and the solid surface modified to reduce the presence of residual silanol groups may be relevant steps. The nature of the solvent on the asymmetric induction is consistent with variations in the location of the complex with respect to the solid–liquid interface and has to be considered and evaluated when developing a heterogeneous catalyst for asymmetric syntheses.

5. Concluding remarks

The easy and reversible inter-conversion between the vanadium oxidation states +IV and +V, the easy formation of peroxido-vanadates, the capacity of vanadium complexes or oxides to act as Lewis acid and basic sites or undergo radical-mediated transformations during catalytic reactions, make vanadium one of the best suited elements for catalytic oxidations and oxygen-transfer reactions, and nature has indeed chosen vanadium for the active site in e.g. vanadium haloperoxidase enzymes.

It has been frequently highlighted, and was also emphasized in the review that one of the major drawbacks of the homogeneous catalysis is the need for separation of the relatively expensive catalysts from the reaction mixture at the end of the process, and that one of the obvious solutions to this separation problem is the use of heterogeneous catalysts.

The catalytic properties of the heterogenized catalysts are sometimes improved compared to the homogeneous ones, this having been mainly ascribed to the contribution of the site-isolation and constraint effects. However, the catalytic behavior of immobilized complexes are invariably more complex than those of their homogeneous counterparts, the immobilization of catalysts often leads to unpredictable changes of catalytic properties, and in fact in most cases the reasons for the better or worse behavior of the immobilized catalysts normally remain unclear. Therefore, as also explicit in this review, although the future may be promising, most results are still far from satisfactory. Notwithstanding, due to the strong limitations of homogeneous catalysis, there is a continuing need to develop more efficient and practical immobilized catalysts, such systems have received a great deal of attention and the trend will certainly continue.

The studies on the influence of support materials on catalysis are very important for the development of more efficient and practical heterogenized chiral catalysts. In this respect, the development of theoretical methods and/or models applicable to e.g. catalysis in nanopores are necessary and would help to further understand the properties of immobilized catalysts and suggest directions for the rational design for more efficient and practical immobilized catalyst systems. Indeed several points should be better understood about reaction mechanisms e.g. in the nanopores. The immobilization of V^{IV}- or V^V-complexes on solids may effectively prevent the formation of inactive dinuclear species, but the selectivity or enan-

tioselectivity effects need to be better understood, namely why they are enhanced or weakened due to the confinement effects inside nanopores e.g. (i) how the surface and the axial grafting modes may affect the coordination of additives to the V centre, (ii) how the reaction microenvironment, including the nanopores and the grafting modes, may have an influence on the stability and lifetime of intermediates, (iii) if the rotation of the intermediate may be greatly retarded by the nanopores compared to the homogeneous reaction conditions, etc.

Immobilization of catalysts on inorganic matrices has several important potential advantages over other approaches such as the use of organic polymer supports. The chemical stability of the inorganic supports is important, particularly with regard to oxidizing conditions. Their mechanical stability is often excellent, since the issue of swelling depending on solvent conditions can largely be avoided. Finally, inorganic supports have superior thermal stability. Indeed, the immobilization of metal ions and metal complexes on inorganic matrices has opened many tracks to more practical fine chemical processes. A serious caveat is, however, the true heterogeneity of several of these new catalytic materials, and side reactions or effects from e.g. the SiOH groups, which normally have a negative impact on selectivity or enantioselectivity. Features of materials such as the effects of particle size, preparation methods, etc., have not been much documented and deserve more attention. In fact, induction of general concepts from scattered cases remains risky.

Polymers, namely polystyrene supported catalysts are still one of the most popular materials as they are not particularly expensive, are readily available, chemically inert and often easy to functionalize. However, the role of the polymeric backbone in the catalytic activity of immobilized metal complexes, or the role of the linker (if used) or the degree of cross-linking is not understood in most cases. Additionally, the polymeric backbone is important for the recycle ability, but sometimes it is either brittle or too rigid, and it can break down after a few uses. Also, polystyrene supports are susceptible to osmotic shock, this breaking down the support as it is washed between uses.

The development of adequate analytical tools that may be applied to the characterization of supported metal complexes has been very important. There are already a wide range of techniques that have been routinely used and were discussed in Section 3. These include solid-state NMR, EPR, electronic, FTIR and Raman spectroscopy, adsorption data, together with elemental analysis and a range of X-ray techniques. EPR has been particularly useful for V^{IV} -immobilized systems, yielding information on the binding set around the V^{IV} -centre in the material. ^{51}V MAS NMR may also give important information for V^V -based catalysts, but has not been much used. It is however fair to say that, despite the potential of the characterization techniques available, there are still gaps that need to be filled and a number of the supported complexes discussed in this review have not been fully characterized. This is of particular concern if the metal complexes are going to be used in catalysis and especially if comparisons are going to be made with “homogeneous analogues”. Also if a supported metal complex is recycled numerous times in catalysis, it is important to know whether the metal complex used in subsequent runs is indeed the same as that prepared and used initially, and if leaching is occurring. This is a relevant issue when they are used in applications such as synthesis of fine chemicals where contamination of the product with heavy metals is highly undesirable.

In conclusion, with the ever-increasing drive to develop more environmentally benign synthetic routes to target compounds, supported vanadium catalysts are becoming increasingly important. New developments are occurring and are proving to be an inspiring and fast growing area, the future perspectives being very exciting.

Acknowledgments

MRM is thankful to Council of Scientific and Industrial Research, New Delhi, and Department of Science and Technology, Government of India, New Delhi for financial support. AK and JCP wish to thank Fundação para a Ciência e a Tecnologia, FEDER and SFRH/BPD/34835/2007 for financial support.

References

- [1] J.H. Clark, D.J. Macquarrie, *Org. Process Res. Dev.* 1 (1997) 149.
- [2] M. Weyand, H.J. Hecht, M. Kiess, M.F. Llaud, H. Vilter, D. Schomburg, *J. Mol. Biol.* 293 (1999) 595.
- [3] J.N. Carter-Franklin, J.D. Parrish, R.A. Tchirret-Guth, R.D. Little, A. Butler, *J. Am. Chem. Soc.* 125 (2003) 3688.
- [4] D. Rehder, *Bioinorganic Vanadium Chemistry*, John Wiley & Sons, New York, 2008.
- [5] A. Butler, *Coord. Chem. Rev.* 187 (1999) 17.
- [6] A. Butler, in: J. Reedijk, E. Bouwman (Eds.), *Bioinorganic Catalysis*, 2nd edn, Marcel Dekker, New York, 1999 (Chapter 5).
- [7] M.J. Clague, N.N. Keder, A. Butler, *Inorg. Chem.* 32 (1993) 4754.
- [8] V. Conte, F. DiFuria, G. Licini, *Appl. Catal. A* 157 (1997) 335.
- [9] A.G.J. Ligtenbarg, R. Hage, B.L. Feringa, *Coord. Chem. Rev.* 237 (2003) 89.
- [10] C. Bolm, *Coord. Chem. Rev.* 237 (2003) 245.
- [11] C.E. Song, *Annu. Rep. Prog. Chem., Sect. C* 101 (2005) 143.
- [12] C.E. Song, S.-G. Lee, *Chem. Rev.* 19 (2002) 3495.
- [13] D.E. De Vos, M. Dams, B.F. Sels, P.A. Jacobs, *Chem. Rev.* 102 (2002) 3615.
- [14] C.A. McNamara, M.J. Dixon, M. Bradley, *Chem. Rev.* 102 (2002) 3275.
- [15] N.E. Leadbeater, M. Marco, *Chem. Rev.* 102 (2002) 3217.
- [16] K.C. Gupta, A.K. Sutar, C.-C. Lin, *Coord. Chem. Rev.* 253 (2009) 1926.
- [17] A.P. Wight, M.E. Davis, *Chem. Rev.* 102 (2002) 3589.
- [18] D.C. Sherrington, *Catal. Today* 57 (2000) 87.
- [19] S. Dzwigaj, *Curr. Opin. Solid State Mater. Sci.* 7 (2003) 461.
- [20] P. McMorn, J. Hutchings, *Chem. Soc. Rev.* 33 (2004) 108.
- [21] C. Li, H.D. Zhang, D.M. Jiang, Q.H. Yang, *Chem. Commun.* (2007) 547.
- [22] R.B. Merrifield, *J. Am. Chem. Soc.* 85 (1963) 2149.
- [23] R. Arshady, G.W. Kenner, A. Ledwith, *Makromol. Chem.* 177 (1976) 2911.
- [24] T.M. Suzuki, T. Yokoyama, *Polyhedron* 2 (1983) 127.
- [25] A. Syamal, M.M. Singh, *Indian J. Chem. Sect. A* 31 (1992) 110.
- [26] A. Syamal, M.M. Singh, *React. Polym.* 21 (1993) 149.
- [27] M.R. Maurya, J. Costa Pessoa, *J. Organomet. Chem.* 696 (2011) 244.
- [28] R. Ando, T. Yagyu, M. Maeda, *Inorg. Chim. Acta* 357 (2004) 2237.
- [29] M.R. Maurya, U. Kumar, I. Correia, P. Adão, J. Costa Pessoa, *Eur. J. Inorg. Chem.* (2008) 577.
- [30] M.R. Maurya, U. Kumar, P. Manikandan, *Dalton Trans.* (2006) 3561.
- [31] M.R. Maurya, U. Kumar, P. Manikandan, *Eur. J. Inorg. Chem.* (2007) 2303.
- [32] M.R. Maurya, A. Arya, U. Kumar, A. Kumar, F. Avecilla, J. Costa Pessoa, *Dalton Trans.* (2009) 9555.
- [33] X.-Q. Yu, J.-S. Huang, W.-Y. Yu, C.-M. Che, *J. Am. Chem. Soc.* 122 (2000) 5337.
- [34] M.R. Maurya, S. Sikarwar, *Catal. Commun.* 8 (2007) 2017.
- [35] M.R. Maurya, M. Kumar, A. Kumar, J. Costa Pessoa, *Dalton Trans.* (2008) 4220.
- [36] L. Canali, D.C. Sherrington, H. Deleuze, *React. Funct. Polym.* 40 (1999) 155.
- [37] M.R. Maurya, M. Kumar, U. Kumar, *J. Mol. Catal. A: Chem.* 273 (2007) 133.
- [38] M.M. Miller, D.C. Sherrington, *J. Catal.* 152 (1995) 368.
- [39] M.R. Maurya, M. Kumar, S. Sikarwar, *React. Funct. Polym.* 66 (2006) 808.
- [40] M.R. Maurya, S. Sikarwar, *J. Mol. Catal. A: Chem.* 263 (2007) 175.
- [41] M.R. Maurya, A. Arya, A. Kumar, J. Costa Pessoa, *Dalton Trans.* (2009) 2185.
- [42] M.R. Maurya, A. Arya, A. Kumar, M.L. Kuznetsov, F. Avecilla, J. Costa Pessoa, *Inorg. Chem.* 49 (2010) 6586.
- [43] M.R. Maurya, A. Arya, P. Adão, J. Costa Pessoa, *Appl. Catal. A: Gen.* 351 (2008) 239.
- [44] M.R. Maurya, M. Kumar, S. Sikarwar, *Catal. Commun.* 10 (2008) 187.
- [45] M. Salavati-Niasari, *J. Incl. Phenom. Macrocycl. Chem.* 65 (2009) 349.
- [46] F. Bedioui, *Coord. Chem. Rev.* 144 (1995) 39.
- [47] K.J. Balkus Jr., A.G. Gabrielov, *J. Incl. Phenom. Mol. Recog. Chem.* 21 (1995) 159.
- [48] M. Salavati-Niasari, M.R. Ganjali, P. Norouzi, *J. Porous Mater.* 14 (2007) 423.
- [49] K.J. Balkus Jr., A.K. Khanamedova, K.M. Dixon, F. Bedioui, *Appl. Catal. A: Gen.* 143 (1996) 159.
- [50] A. Kozlov, K. Asakura, Y. Iwasawa, *Microporous Mesoporous Mater.* 21 (1998) 571.
- [51] T. Joseph, D. Srinivas, C.S. Gopinath, S.B. Halligudi, *Catal. Lett.* 83 (2002) 209.
- [52] A.P.A. Marques, E.R. Dockal, F.C. Skrobot, I.L.V. Rosa, *Inorg. Chem. Commun.* 10 (2007) 255.
- [53] M.R. Maurya, H. Saklani, S. Agarwal, *Catal. Commun.* 5 (2004) 563.
- [54] M.R. Maurya, A.K. Chandrakar, S. Chand, *J. Mol. Catal. A: Chem.* 263 (2007) 227.
- [55] M.R. Maurya, A.K. Chandrakar, S. Chand, *J. Mol. Catal. A: Chem.* 270 (2007) 225.
- [56] M.R. Maurya, A.K. Chandrakar, S. Chand, *J. Mol. Catal. A: Chem.* 274 (2007) 192.
- [57] M.R. Maurya, A.K. Chandrakar, S. Chand, *J. Mol. Catal. A: Chem.* 278 (2007) 12.

- [58] M.R. Maurya, M. Kumar, S.J.J. Titinchi, H.S. Abbo, S. Chand, *Catal. Lett.* 86 (2003) 97.
- [59] M.R. Maurya, H. Saklani, A. Kumar, S. Chand, *Catal. Lett.* 87 (2004) 121.
- [60] S. Seelan, A.K. Sinha, *Appl. Catal. A: Gen.* 238 (2003) 201.
- [61] M. Salavati-Niasari, *Inorg. Chim. Acta* 362 (2009) 2159.
- [62] P.P. Knops-Gerrits, C.A. Trujillo, B.Z. Zhan, X.Y. Li, P.A. Jacobs, *Top. Catal.* 3 (1996) 437.
- [63] T.A. Fernandes, C.D. Nunes, P.D. Vaz, M.J. Calhorda, P. Brandao, J. Rocha, I.S. Goncalves, A.A. Valente, L.P. Ferreira, M. Godinho, P. Ferreira, *Microporous Mesoporous Mater.* 112 (2008) 14.
- [64] T. Joseph, S.B. Halligudi, *J. Mol. Catal. A: Chem.* 229 (2005) 241.
- [65] T. Joseph, M. Hartmann, S. Ernst, S.B. Halligudi, *J. Mol. Catal. A: Chem.* 207 (2004) 131.
- [66] K.M. Parida, S. Singha, P.C. Sahoo, *J. Mol. Catal. A: Chem.* 325 (2010) 40.
- [67] C.-H. Lee, T.S. Lin, C.Y. Mou, *J. Phys. Chem. B* 107 (2003) 2543.
- [68] J.Q. Zhao, W.Y. Wang, Y.C. Zhang, *J. Inorg. Organomet. Polym. Mater.* 18 (2008) 441.
- [69] C. Baleizao, B. Gigante, H. Garcia, A. Corma, *J. Catal.* 215 (2003) 199.
- [70] A. Fuerte, M. Iglesias, F. Sánchez, A. Corma, *J. Mol. Catal. A: Chem.* 211 (2004) 227.
- [71] X.S. Zhao, F. Su, Q. Yan, W. Guo, X.Y. Bao, L. Lv, Z. Zhou, *J. Mater. Chem.* 16 (2006) 637.
- [72] P.T. Tanev, T.J. Pinnavaia, *Science* 267 (1995) 865.
- [73] K. Wilson, J.H. Clark, *Pure Appl. Chem.* 72 (2000) 1313.
- [74] C. Pereira, A.R. Silva, A.P. Carvalho, J. Pires, C. Freire, *J. Mol. Catal. A: Chem.* 283 (2008) 5.
- [75] B. Jarrais, C. Pereira, A.R. Silva, A.P. Carvalho, J. Pires, C. Freire, *Polyhedron* 28 (2009) 994.
- [76] A.-M. Hanu, S. Liu, V. Meynen, P. Cool, E. Popovici, E.F. Vansant, *Microporous Mesoporous Mater.* 95 (2006) 31.
- [77] M. Baltes, O. Collart, P. Van der Voort, E.F. Vansant, *Langmuir* 15 (1999) 5841.
- [78] A. Lattanzi, N.E. Leadbeater, *Org. Lett.* 4 (2002) 1519.
- [79] B. Jarrais, A.R. Silva, C. Freire, *Eur. J. Inorg. Chem.* (2005) 4582.
- [80] L.F.B. Malta, J.D. Senra, M.E. Medeiros, O.A.C. Antunes, *Supramol. Chem.* 18 (4) (2006) 327.
- [81] P. Arroyo, S. Gil, A. Munoz, P. Palanca, J. Sanchos, V. Sanz, *J. Mol. Catal. A: Chem.* 160 (2000) 403.
- [82] M.R. Maurya, S. Sikarwar, T. Joseph, P. Manikandan, S.B. Halligudi, *React. Funct. Polym.* 63 (2005) 71.
- [83] M.R. Maurya, S. Sikarwar, P. Manikandan, *Appl. Catal. A: Gen.* 315 (2006) 74.
- [84] V. Pärvulescu, C. Anastasescu, B.L. Su, *J. Mol. Catal. A: Chem.* 198 (2003) 249.
- [85] H.M. Alvarez, L.F.B. Malta, M.H. Herbst, A. Horn, O.A.C. Antunes, *Appl. Catal. A: Gen.* 326 (2007) 82.
- [86] A. Kozlov, A. Koslova, K. Asakura, Y. Iwasawa, *J. Mol. Catal. A: Chem.* 137 (1999) 223.
- [87] S. Brunauer, P.H. Emmett, E. Teller, *J. Am. Chem. Soc.* 60 (1938) 309.
- [88] S.J. Gregg, K.S.W. Sing, *Adsorption, Surface Area and Porosity*, 2nd ed., Academic Press, London, 1982.
- [89] C. Li, *Catal. Rev.* 46 (2004) 419.
- [90] D.C. Sherrington, in: J.H. Clark (Ed.), *Chemistry of Waste Minimisation*, Blackie Academic, London, 1995 (Chapter 6).
- [91] C.Y. Chen, S.-Q. Xiao, M.E. Davis, *Microporous Mater.* 4 (1995) 1.
- [92] V. Alfredsson, M. Keung, A. Monnier, G.D. Stucky, K.K. Unger, F. Schüth, *J. Chem. Soc., Chem. Commun.* (1994) 921.
- [93] W. Li, L. Luo, H. Yamashita, J.A. Labinger, M.E. Davis, *Microporous Mesoporous Mater.* 37 (2000) 57.
- [94] L.F. Vilas Boas, J. Costa Pessoa, in: G. Wilkinson, R.D. Gillard, J.A. Mc Cleverty (Eds.), *Comprehensive Coordination Chemistry*, Pergamon, Oxford, 1987, p. 453.
- [95] M. Sívák, H. Gécilová, *Acta F. R. N. Univ. Comen. Chimia* 35 (1987) 81.
- [96] E. Bastardo-Gonzalez, W. Jones, K. Bahrnowski, M. Labanowska, E.M. Serwicka, *Microporous Mesoporous Mater.* 50 (2001) 51.
- [97] K. Würthrich, *Helv. Chim. Acta* 48 (1965) 1012.
- [98] N.D. Chasteen, in: J. Reuben (Ed.), *Biological Magnetic Resonance*, Plenum, New York, 1981, p. 53.
- [99] G. Martini, M.F. Ottaviani, G.L. Seravalli, *J. Phys. Chem.* 79 (1975) 1716.
- [100] R.A. Sheldon, *Bull. Soc. Chim. Belg.* 94 (1985) 651.
- [101] R. De la Rosa, M.J. Clague, A. Butler, *J. Am. Chem. Soc.* 114 (1992) 760.
- [102] T.A. Alsalm, J.S. Hadi, E.A. Al-Nasir, H.S. Abbo, S.J.J. Titinchi, *Catal. Lett.* 136 (2010) 228.
- [103] T.E. Müller, M. Beller, *Chem. Rev.* 98 (1998) 675.
- [104] V. Hulea, E. Dumitriu, *Appl. Catal. A: Gen.* 277 (2004) 99.
- [105] H.M. Alvarez, L.F.B. Malta, M.H. Herbst, A. Horn Jr., O.A.C. Antunes, *Appl. Catal. A: Gen.* 326 (2007) 82.
- [106] J.D. Koola, J.K. Kochi, *J. Org. Chem.* 52 (1987) 4545.
- [107] W. Nam, R. Ho, J.S. Valentine, *J. Am. Chem. Soc.* 113 (1991) 7052.
- [108] A.H. Heines, *Methods for the Oxidation of Organic Compounds*, Academic Press, London, 1985.
- [109] A.T. Radosevich, C. Musich, F.D. Toste, *J. Am. Chem. Soc.* 127 (2005) 1090.
- [110] S.-S. Weng, M.-W. Shen, J.-Q. Kao, Y.S. Munot, C.-T. Chen, *Proc. Natl. Acad. Sci. U.S.A.* 103 (2006) 3522.
- [111] C.-T. Chen, S. Bettigeri, S.-S. Weng, V.D. Pawar, Y.-H. Lin, C.-Y. Liu, W.-Z. Lee, *J. Org. Chem.* 72 (2007) 8175.
- [112] R.A. Shiels, K. Venkatasubbaiah, C.W. Jones, *Adv. Synth. Catal.* 350 (2008) 2823.